SET3901-THESIS PROJECT

Lab Scale optimization and characterization of Aluminium and TCO layer for flexible thin film solar modules

TU Delft Delft University of Technology

Lab Scale Optimization and Characterization of the aluminium and TCO layer for flexible thin film solar modules

by

Rajat Subramanian

to obtain the degree of Master of Science
at the Delft University of Technology,
to be defended publicly on Friday August 19, 2022 at 01:00 PM.

Student number:	5269679	
Project duration:	November 1, 2021 - August 19, 2022	
Thesis committee:	Prof. dr. ir. Arno Smets,	TU Delft,ESE-PVMD, supervisor
	Dr. Gianluca Limodio,	TU Delft,ESE-PVMD, daily supervisor
	Prof. dr. ir. Aditya Shekhar,	TU Delft,ESE-DCE&S
	Mohammed El Makkaoui,	HyET Solar, company Supervisor

HyET Solar
Flexible light weight solar modules

TU Delft Delft University of Technology

PVMD
Delft University of Technology

Acknowledgement

The past two years has been nothing short of a roller coaster ride, from tackling all the subjects in my first year to doing my internship and thesis in the second year. It was further challenging due to the COVID-19 pandemic, because of which my education was online for most of my first year.Overall, the experience of doing my masters at TU Delft has been a cherisable one, with memories and experiences which will help me in overcoming future challenges.

I would first like to take the opportunity to thank Professor Dr. Arno Smets for providing me the opportunity to work under his supervision and connecting me with HyET Solar in Arnhem. I have always been interested in working under him, and I saw his MOOCs on solar energy which motivated me to pursue my masters in TU Delft. I would also like to take this oppurtunity to thank Dr. Gianluca Limodio for his guidance and supervision during both my internship as well as my thesis. He was always willing to share his knowledge with me and was always there to clear my doubts.

I would also like to thank Mohammed El Makkaoui as well as Dr. Jimmy Melskins for guiding me through my thesis project. They were always there to assist me whenever I faced any obstacles during my time at HyET. They were always friendly and never hesitated to clear my doubts. I would also like to thank all the people at HyET Solar especially Edward Hamers, Herbert Lifka and Remco Regling with whom I had enjoyed several insightful and great discussions. All the people at HyET Solar were very approachable and friendly and they were always there to solve my queries. I would also like to thank my seniors Achinth, Rajesh and Rahul for their constant support and guidance throughout my thesis.

Last but not the least, I would like to my family for their constant support and guidance throughout my time as master student at TU Delft. They were always there to encourage me and really helped me overcome my home sickness. I would like to once again thank them for providing my the opportunity to do my masters in the Netherlands which overall has given me experiences to cherish for a lifetime. I hope to carry on from my masters journey and work towards the development of sustainable energy in the coming years.

Rajat Subramanian
19th August 2022

Abstract

This work is part of the FLAMINGO PV group which is a joint partnership between TU Delft and HyET Solar, which aims to demonstrate efficiencies above 12% on tandem thin film silicon devices. This thesis focused on the optimization of the aluminium surface morphology as well as the TCO layer at HyET Solar.In order to achieve the desired objectives of the FLAMINGO PV group, it is essential to optimize these layers in order to ensure better device performance for the HyET Solar modules.

Overall, in this thesis, a reliable and efficient method for the characterization of the TCO at HyET Solar has been established which makes it easier to determine whether the TCO exhibits desired electrical and structural properties. An experiment was performed in which different TCO thicknesses were varied in order to determine the optimal thickness for the new aluminium foil at HyET. Overall, thicknesses of 750-790 nm were found to yield desired TCO characteristics.

Furthermore, the thesis also focused in addressing the issues regarding the precipitants which occurred as a result of the treatment process which aims to remove oil/grease and other surface impurities from the aluminium substrate. The focus of this project was to address the precipitants issue which could hinder the performance of the current HyET modules. Overall, ultrasonication appeared to be the method for the removal of the precipitants. Different acids were tried among which H_3PO_4 and HNO_3 were found to be the most optimal for removing the precipitants when the samples were dipped in them for atleast 3 minutes. Confirmation tests with different HyET textures need to be implemented however to confirm their presence.

Overall, through this thesis, the electrical and structural properties of the TCO layer at HyET was studied and the optimal thickness of 750-790 nm was selected based on their relatively good structural and electrical performance. Also, the precipitants issue has been tackled with ultrasonication with acids such as H_3PO_4 and HNO_3 proving to be the best bet so far for eliminating them.

Contents

List of Figures

List of Tables

1

Introduction

This chapter aims to emphasize the importance of renewable energy, especially solar energy to fulfill our energy needs.Section 1.1 introduces the world of solar photovoltaics.Section 1.2 talks about the different types of solar cells, including the thin film solar technology which is the focus for this thesis.Sections 1.3 and 1.4 describe in detail the thin film solar technology as well as the company HyET Solar, where I pursued my thesis.Finally sections 1.5 and 1.6 describe the FLAMINGO PV project in the context of which I did my thesis as well as the aims and outlines of my thesis.

Solar energy is defined as the energy harnessed from the sun in order to produce electricity. The radiant heat and the energy of the sun is also used for producing solar thermal energy which is used in various applications such as solar heating and solar architecture [1, 2].

Solar energy technologies can be divided into active or passive solar depending on the way they utilize or harness the energy from the sun. Active solar photovoltaics directly harness the energy from the sun and comprise of concentrated solar photovoltaics, photovoltaic systems and solar water heating [1, 2]. Meanwhile, passive solar techniques harness the energy from the sun indirectly and they mainly comprise of building integrated solar photovoltaics(BIPV). In recent years, solar energy has been much more cost effective which has significantly led to its rise in recent years. Figure 1.1 shows the exponential rise witnessed in solar photovoltaics since the turn of the 21st century [3, 4].

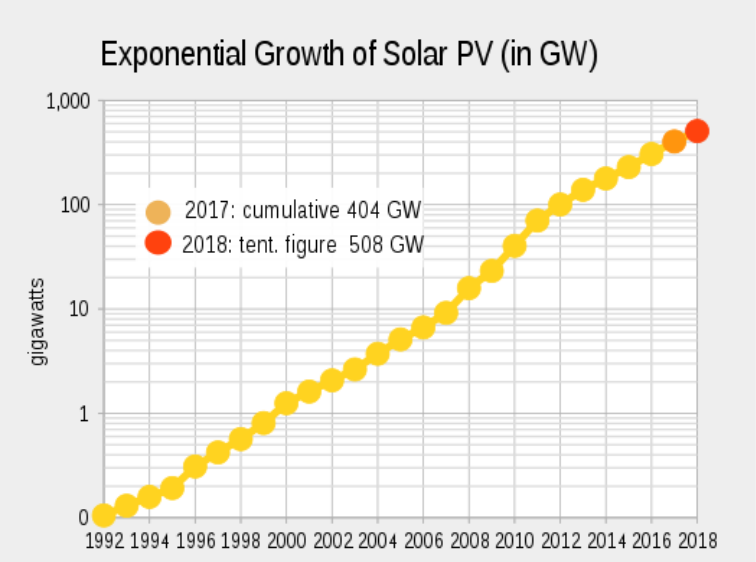

Figure 1.1: Growth of Solar Photovoltaics globally from 2003-2018 [5]

1.1. Introduction to Solar Photovoltaics

A solar cell, or photovoltaic cell, is an electrical device that converts the energy of the sun directly into electricity which is known as the photovoltaic effect.Its electrical properties such as current, voltage or resistance vary significantly when exposed to any form of light. Solar cells are the building blocks and collection of these solar cells lead to formation of solar modules or solar panels [6]. The operation of a photovoltaic (PV) cell requires 3 basic attributes [6]:

1. The absorption of light, which lead to generation of electron-hole pairs.
2. The separation of positive and the negative charge carriers
3. The separate collection of these carriers at the terminals of the cell

1.2. Types of Solar Cells:

The following subsections will explain about the different types of solar cells. Based on the material used for their production, they have been classified as first generation, second generation and third generation depicted by the subsections respectively.

1.2.1. First Generation Solar Cells:

First generation solar cells are highly developed in terms of their deployment and their fabrication. They include mostly crystalline silicon solar cells, which have been preferred for several years. Crystalline silicon solar cells can be further classified into monocrystalline and polycrystalline solar cells [6, 7, 8]. Mono crystalline solar cells are manufactured from single crystals of silicon by the Czochralski process during which the silicon crystals are sliced from big ingots [9, 10, 11]. The typical efficiencies of crystalline silicon solar cells lie between 18% - 22% [12]. Its drawbacks however, are that their processing requires extensive precision and it is more expensive compared to other silicon technologies since only one type of crystal is used for every cell. Polycrystalline PV modules, on the other hand consist of crystal grains which are separated from each other with the help of grain boundaries.The processing of polycrystalline silicon solar cells are produced by cooling a graphite mould which contains molten silicon [13].Figure 1.2 below shows the first generation solar cells.

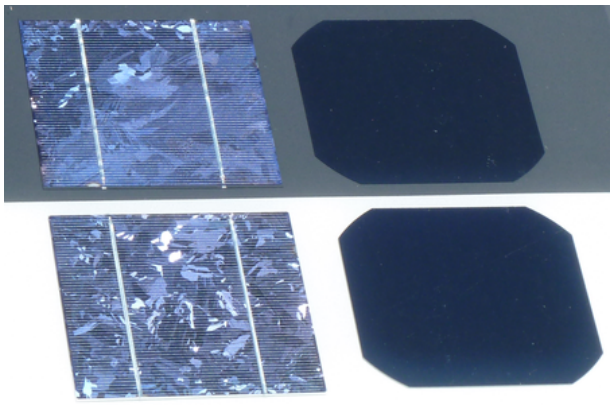

Figure 1.2: First Generation polycrystalline silicon solar cell, polycrytalline silicon(left) and monocrystalline silicon(right)[5]

1.2.2. Second Generation Solar Cells:

Most of the thin film solar cells constitute the second generation solar cells, which have thinner layers usually around 1 µm thick and are hence less expensive compared to their first generation counterparts. Thin film solar cells are classified as follows [14]:

- Thin film silicon solar cells
- cadmium telluride(CdTe)
- copper indium gallium diselenide(CIGS)

Thin film silicon solar PV modules are much more preferred compared to other second generation solar modules as they are much more economical and offer better stability at higher temperatures. Thin film silicon solar cells are manufactured by the plasma enhanced chemical vapor deposition process(PECVD) which enables it to be manufactured at lower temperatures thereby resulting in a large reduction of input energy. Another advantage of thin film solar cells is that they can be deposited on flexible substrates and can even generate electricity even in bad weather conditions [15]. One of the leading companies in amorphous silicon solar technology is HyET Solar in Arnhem, Netherlands where I have pursued my master thesis and its technology will be the point of focus for this thesis. Figure 1.3 below highlights the thin film silicon which falls under the category of second generation thin film solar cells.

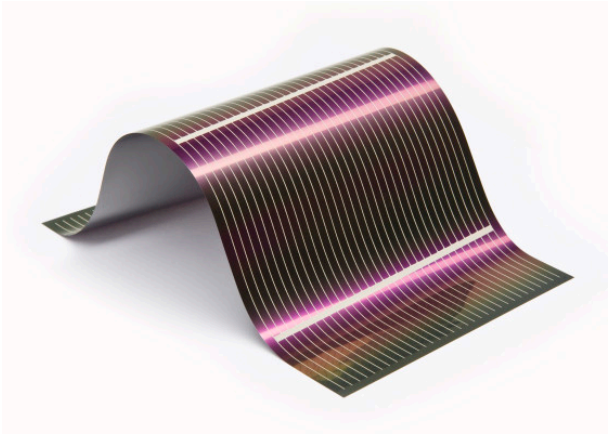

Figure 1.3: Thin film silicon solar cells[16]

1.2.3. Third Generation Solar Cells:

Third-generation photovoltaic cells are solar cells which are currently in the research and developmental phase. These solar cells are exciting as they have the ability to come close to the Shockley–Queisser limit of 31–41% power efficiency for single band-gap solar cells [17, 18]. Emerging third generation solar photovoltaics include:

1. Copper zinc tin sulfide solar cell (CZTS)
2. Dye-sensitized solar cell
3. Organic solar cell
4. Quantum dot solar cell
5. Perovskite solar cell

Perovskite solar cells, in particular has received a lot of attention in recent years as it has demonstrated efficiencies above 20 percent. In addition to that, they are also easy to produce, require thinner layers of materials and are cost effective [19, 20].Figure 1.4 below depicts the organic solar cells which fall under the category of third generation solar cells.

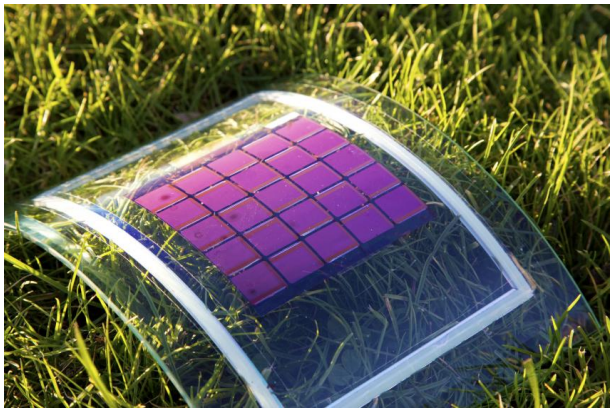

Figure 1.4: Organic Solar cell [21]

1.3. Introduction to thin film solar cells

Thin film solar cells are produced through the deposition of one or more thin layers of PV materials on a substrate such as glass or metal. Thin film solar technologies include perovskites, cadmium telluride (CdTe), copper indium gallium selenide (CIGS), and thin-film silicon.

The thickness of the layers varies from a few nanometers (nm) to tens of micrometers (µm), and is much thinner compared to the currently used crystalline silicon solar cell (c-Si), which consists of layers up to 200 µm thick [22]. Hence, this ensures that thin film solar cells consume less material, can be deposited on flexible substrates and are lightweight. Thus, thin film solar cells are preferred in several applications especially in the field of building-integrated photovoltaics (BIPV) [23].

However, despite these advantages, the thin-film technology has always been less efficient compared to its c-Si counterpart. The declining prices of c-Si in recent years has further declined the use of thin film solar cells. Its lifetime is usually expected to be at least 20 years for it to be competitive in the market. However, thin film solar modules have great advantages as mentioned above and has a high potential to change the PV landscape in the coming years [22]. This thesis will focus on the thin film silicon modules produced at HyET Solar. Figure 1.5 depicts the layers of the thin film solar cell at HyET Solar.

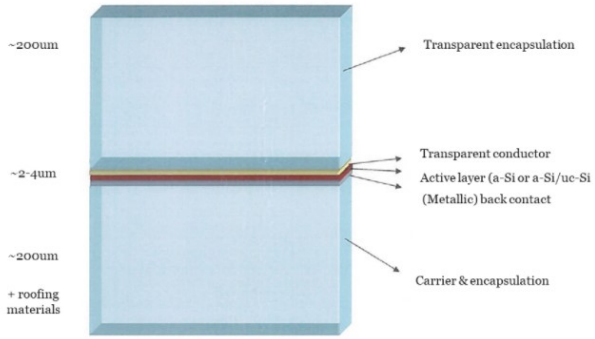

Figure 1.5: Different layers of the thin film solar cell at HyET Solar [23]

1.4. About the Company HyET Solar

This section emphasizes on the company HyET Solar and its production process for thin film a-silicon solar modules. Section 1.4.1 below provides a brief overview of the company HyET Solar and its history. Section 1.4.2 focuses on the production process of the thin film solar modules at HyET Solar.

1.4.1. Overview of HyET Solar

The company HyET Solar is located in Arnhem in the east of the Netherlands. It was formed in June 2012 after it took over the assets and the knowledge of the former company Helianthos. Helianthos started in 1997 which branched out from Akzo Nobel, and it formed a partnership with Akzo Nobel and Shell from 2001 till 2006. In 2006, it was then taken over by Nuon. Apart from R & D labs, HyET Solar also consists of a small-scale 1 MW production plant for the Roll-to-Roll production of flexible a-Si:H and a-Si:H/nc-Si:H tandem solar modules. The main advantage of these modules is that it is cost effective and easier to produce in a larger scale compared to the crystalline silicon solar modules which are largely used today. It is also lightweight, uses less material and can also perform better at higher temperatures. HyET is taking big strides to fulfil the potential of amorphous silicon solar modules and plans to expand the production capacity to 40 MW in the near future.Figure 1.6a and 1.6b below show the production facility of HyET Solar in Arnhem as well as the thin film silicon solar modules produced there [24].

(a) Production Facility of HyET Solar [25]

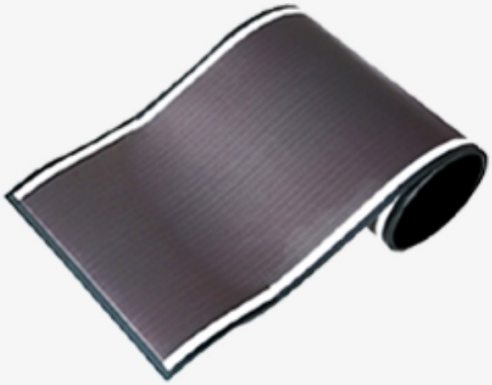

(b) Thin film silicon solar module produced at HyET [26]

Figure 1.6: Overview of HyET Solar in Arnhem

1.4.2. Production Process

The production process in the HyET Solar plant is a sequence of Roll-to-Roll process steps. Bare aluminum foil is used as a temporary carrier for the deposition processes due to its low cost and its good stability at higher temperatures required for the deposition processes. Afterwards, the deposition of a front transparent conductive oxide (TCO) layer on the aluminum through the APCVD (atmospheric pressure chemical vapor deposition) process. HyET desires a TCO layer which is highly transparent and conductive in nature to ensure the production of highly efficient modules. Due to its low cost, desirable characteristics and high stability,fluorine based tin oxide(FTO) is used as the TCO layer at HyET Solar.Also, a trade-off is kept between the electrical and the optical parameters of the TCO in order to ensure the TCO satisfies both these characteristics. The next step involves deposition of the silicon layers through the PECVD (plasma enhanced chemical vapor deposition) process. Afterwards, the foil is divided in individual cell through monolithic interconnection which is done through laser scribing. Then, the back contact, consisting of a layer of ZnO and a layer of Al is sputtered onto the Al substrate. Next steps involve the lamination of the foil with the help of a permanent plastic carrier(PEN). Following the lamination process is the etching step which removes the temporary aluminum carrier.The modules are then encapsulated to protect the solar cells from external parameters such as rain, high heat etc.Lastly, quality control is carried out to ensure proper functioning of the modules [24]. The production process of HyET Solar is depicted in figure 1.7 below.

Figure 1.7: Production process for a-Si modules at HyET Solar [27]

1.5. Flamingo PV

FLAMINGO PV stands for flexible, lightweight, advanced materials in next generation of photovoltaics. It is a collaboration between TU Delft and HyET Solar B.V which aims to develop flexible tandem thin film solar modules with efficiencies above 12% and a high lifetime of around 35 years. The main advantages of this technology are that it offers low cost,high energy yield as well as easy scalability.Due to their flexible nature, they also find great use in building integrated photovoltics(BIPV).Also, the use of materials such as fluorine doped tin oxide ensure greater reliability and lower costs overall for the modules [9]. Currently, the single junction a-Si:H modules at HyET demonstrate efficiencies of around 7-8% . Tandem modules which contain a-Si:H and nc-Si:H are currently in development at HyET which have the potential to demonstrate 12% efficiencies.These modules are produced using the roll to roll technology. HyET currently operates with 35cm wide aluminium foil as the temporary substrate and aims to use wider aluminium foils of around 130 cm in the near future. The process makes use of 110 micron aluminum foil as a substrate during the deposition of the TCO as well as the silicon layers which is later etched away and replaced by a permanent plastic carrier. FLAMINGO PV aims to demonstrate 12% stabilized efficiency on tandem devices and 14% stabilized efficiency on triple junction devices on lab scale. This technology will later be realized in the production line with the aim of achieving 12% efficiency on the roll to roll production of flexible thin film solar modules [28].

1.6. Aim and Outline of Thesis

This thesis is part of the FLAMINGO PV project. This thesis aims to optimize the lab-scale production process of the HyET Solar modules in order to demonstrate the desired efficiencies of 12% . This thesis focuses on the development of an effective means to characterize/qualify the TCO. This thesis also lays emphasis on addressing the issues regarding the imperfections in the HyET aluminium foil (milling tracks and holes of the as received foil and precipitants that arise after pre-treatment) which are undesirable and may have a negative impact on the deposition of the TCO. This could ultimately influence the solar cell performance and introduce undesirable effects, such as shunts. Therefore, it is important to understand the effects of these defects on performance and determine how to they can be addressed.Finally, results from the TCO experiments were taken in order to make better working lab modules. The aims of the thesis is further discussed below:

- Establish a method for efficient characterization of the TCO layer at HyET Solar
- Determination of the ideal TCO thickness which demonstrates great electrical and structural properties of the TCO desired by HyET.
- Optimize the pre-treatment process at HyET Solar in order to ensure a lower concentration of defects such as holes or precipitants on the aluminium substrate.
- Address the issue regarding the precipitants.

The report is structured as follows: Chapter 1 gives a brief introduction regarding solar photovoltaics as well as provides a basic overview of the thin film silicon solar modules produced at HyET Solar. Chapter 2 focuses mainly on the solar cell principles as well as discusses the solar cell parameters. It also focuses on the solar cell losses as well as the strategies which could be implemented in order to mitigate them. Chapter 3 provides an overview of the TCO layer in solar cells. It also lays its emphasis on the TCO used at HyET Solar as well as the different characterization measurements used to judge its performance. Chapter 4 mainly focuses on the TCO thickness variation experiments including the main observations and conclusions obtained from performing the experiment. Chapter 5 mainly focuses on addressing the issues regarding the presence of precipitants on HyET aluminium foil. Chapter 6 lays emphasis on the lab scale production of solar modules based on the results from the TC thickness experiment. Lastly, chapter 7 focuses on the overall conclusions gained from this thesis project as well as the future work which could be implemented in order to achieve better performance from the HyET modules.

2

Solar Cell fundamentals

This chapter provides information regarding the basic solar cell fundamentals.Section 2.1 discusses the basic working principle of solar cells.Section 2.2 talks about the essential parameters which help to quantify the solar cell performance.Sections 2.3 and 2.4 describe the solar cell optics and the solar cell losses respectively.Finally section 2.5 discusses the strategies which can be implemented to prevent losses in solar cells.

2.1. Solar Cell Working Principle

Solar cells operate with the process known as the photovoltaic effect, which forms a potential difference across the junction of two different materials. The potential difference occurs because of the electromagnetic radiation and performs work when the external circuit is connected. This effect was explained by Albert Einstein in 1905 by assuming light contains photons, which are well defined energy quanta [29]. The energy of a photon is given by:

$$E = h\upsilon \tag{2.1}$$

Where E is the energy of the photon, h is the Plank's constant, and υ is the electromagnetic frequency. The photovoltaic effect can be divided into three main processes [29]:

- Generation of charge carriers due to photon absorption: When a photon is absorbed in the material, its energy excites the electron from an initial energy level (E_i) to a higher energy level (E_f) whose difference gives the photon energy. In a typical semiconductor, the electrons are located below the valence band (E_v)) and above the conduction band (E_c). The bandgap (E_G) represents the difference between these two bands which are devoid of any energy states between them. A photon must have minimum energy of E_G to get absorbed. When an electron is excited from E_i to E_f, a void is created at the initial energy level which are defined as holes [29].

- Separation of photo-generated charge carriers: To utilize the energy stored in an electron-hole pair for external work, it is necessary to ensure that semi-permeable membranes are present which ensure separate movement of holes and electrons across their ends. Hence, it is essential to ensure smooth movement of the holes and electrons to their respective membranes before they recombine with each other [29].

- Collection of photo-generated charge carriers: In order to perform work, the charge carriers are extracted and collected at the ends of the terminals where the chemical energy of the charge carriers are converted to electrical energy. Afterwards, the electron hole pair recombines at the metal absorber interface [14]. The working principle of solar cell is given below in figure 2.1 as follows [29]:

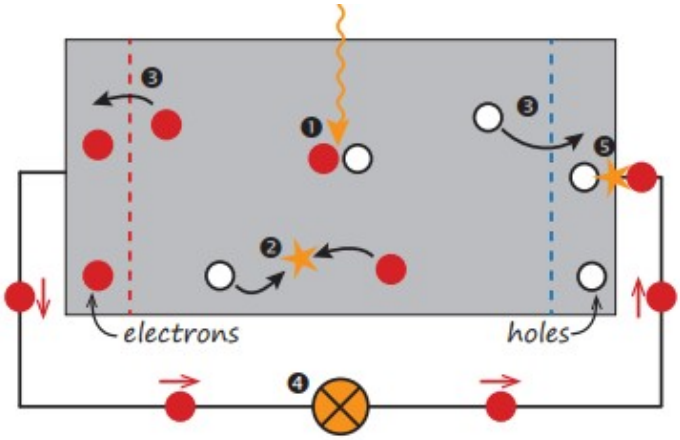

Figure 2.1: Working Principle of solar cells highlighting (1) The generation of charge carriers (2) Separation of the charge carriers (3) Collection of the charge carriers across the ends of the terminals of the solar cell [29]

2.2. Solar Cell Parameters

To judge and compare the solar cells, a predefined set of parameters are used for their quantification. These parameters are measured under standard test conditions i.e cell temperature of 25°C , 1000 W/m^2 irradiance and AM 1.5 spectrum. These conditions are essential for ensuring reliable comparison between the different solar cells. The parameters used for determining the performance of a solar cell are as follows [29]:

- Open circuit voltage: Open circuit voltage is defined as the voltage at which no current is flowing across the ends of the external circuit. This is also the maximum voltage which can be exhibited by the solar cell. Photogenerated current density helps significantly in determination of the open circuit voltage [29].

- Short circuit current: Short circuit current is defined as the current flowing through the external circuit in case of short circuit in the electrodes of the solar cell. Photon flux plays an important role in short circuit voltage, which is further dependent on the spectrum of the incident light [14].

- Fill factor: Fill factor is defined as the ratio of the maximum power which can be extracted from a solar cell to the product of the open circuit voltage and the short circuit current. It is desirable to have solar cells with a fill factor greater than 0.8. The equation for the fill factor is shown below as follows [29]:

$$FF = \frac{J_{mpp} * V_{mpp}}{J_{sc} * V_{oc}} \tag{2.2}$$

  where the 'mpp' refers to the maximum power-point. To obtain desirable efficiencies, it is recommended to operate the solar cell at the maximum power-point.

- Conversion efficiency: Conversion efficiency is defined as the ratio of maximum generated power to that of the incident power [29].

$$\eta = P_{max} * I_{in} = J_{mpp} * V_{mpp} * I_{in} = \frac{J_{sc} * V_{oc} * FF}{I_{in}} \tag{2.3}$$

- External quantum efficiency: External quantum efficiency (EQE) is defined as the fraction of photons which are collected at the terminals of the cell which can generate electron hole pairs in the absorber layer. The EQE depends highly on the wavelength of incident light.

$$EQE(\lambda) = I_{ph}(\lambda) * q * \Psi_{ph,\lambda} \tag{2.4}$$

  where the elementary charge is denoted by 'q', $\Psi_{ph,\lambda}$ is the spectral photon flux, λ is the wavelength and I_{ph} is the photo-current.

2.3. Solar cell Optics

Efficient absorption of the light by the solar cell is one process crucial to obtain high power and efficiency. An ideal solar cell is the solar cell which can absorb 100% of the incident light and convert into useful energy, however in reality, the optical capabilities and other losses inhibit 100% use of the incident light. The optical capabilities of the solar cell depend on the properties as well as the behaviour of the light. The speed of light varies from one medium to another. This is characterized by the refractive index, which is the ratio of the speed of light in a vacuum to the speed of light in the medium [29].

2.3.1. Optics of flat interfaces

Two mediums, m_1 & m_2 are considered in this study. The two media are non-absorptive in nature and consist of only the real parts of the refractive indices, namely n_1 & n_2 respectively. A part of the incident light is reflected at the boundary whereas the other part is either refracted or transmitted. The incident light as well as the reflected and transmitted light is depicted below in figure 2.2. According to the law of reflection, the angle of incident light is equal to the angle of the scattered light [29]:

$$\theta_i = \theta_r \tag{2.5}$$

where θ_r is the angle of scattered light and θ_i is the angle of incident light.Snell's law is used to describe the relation between refracted light and incident light which is given below as follows:

$$n_1 \sin\theta_i = n_2 \sin\theta_t \tag{2.6}$$

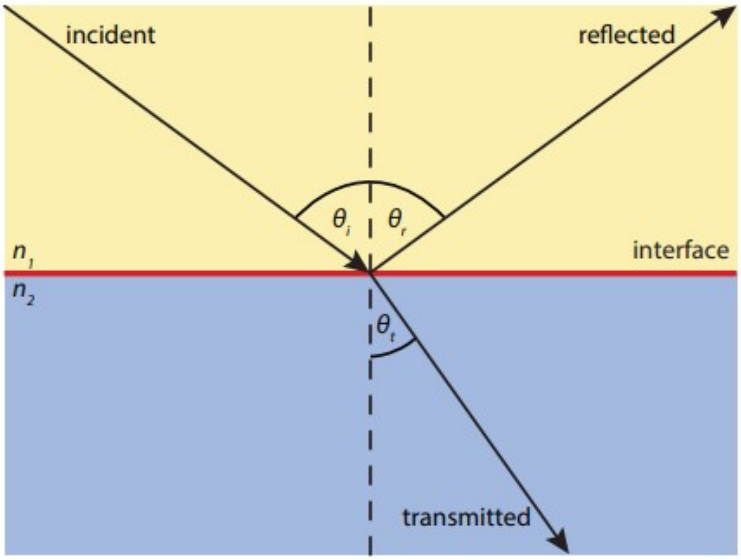

Figure 2.2: Solar cell optics on a flat surface with the incident, reflected and transmitted light paths [29]

Fresnel equations helps to correlate the magnitudes of the incident, refracted, and reflected light. The polarized light plays a significant influence on the electric field which can be either be parallel or perpendicular to the plane of incidence. The Fresnel equations for perpendicular polarized light denoted by 's' is given by [29]:

$$t_s = \left(\frac{\xi_{0t}}{\xi_{0i}}\right) = \frac{2n_1 \cos\theta_i}{n_1 \cos\theta_i + n_2 \cos\theta_t} \tag{2.7}$$

$$t_s = \left(\frac{\xi_{0r}}{\xi_{0i}}\right) = \frac{n_1 \cos\theta_i - n_2 \cos\theta_t}{n_1 \cos\theta_i + n_2 \cos\theta_t} \tag{2.8}$$

The Fresnel equations for parallel polarized light denoted by 'p' is as follows:

$$t_s = \left(\frac{\xi_{0t}}{\xi_{0i}}\right) = \frac{2n_1 \cos\theta_i}{n_1 \cos\theta_i + n_2 \cos\theta_t} \tag{2.9}$$

$$t_s = (\frac{\xi_{0r}}{\xi_{0i}}) = \frac{n_1 \cos\theta_t - n_2 \cos\theta_i}{n_1 \cos\theta_i + n_2 \cos\theta_t} \tag{2.10}$$

For unpolarized light, the mean value of the two polarizations are taken. Therefore, the equation for the overall reflection from a solar cell is given below as follows:

$$R = \frac{1}{2}(r_s^2 + r_p^2) \tag{2.11}$$

At normal incidence, the angle of incidence, i.e θ_i = 0. From the law of conservation of energy, the sum or reflectance and transmittance must be equal to unity [29]. Therefore, the equation for the transmittance of a solar cell is highlighted below as follows:

$$T = 1 - R = \frac{n_2 \cos\theta_t}{n_1 \cos\theta_i}\frac{1}{2}(t_s^2 + t_p^2) \tag{2.12}$$

From Snell's law, if the refractive index of material 2 is greater than material 1, i.e n2 > n1, there is an angle called critical angle above which light will not leave the layer with n2. This is when the phenomena of total internal reflection takes place. The equation for the critical angle is given as follows [29]:

$$\sin\theta_{crit} = \frac{n_1}{n_2} \tag{2.13}$$

2.3.2. Optics in Absorptive Media

The solar cell works on the principle of light absorption in the absorber layer which excites the charge carriers which are then used to generate electric current [14]. The optical properties of the solar cell plays a major role in the intensity of light travelling through the absorber layer.The optical properties of an absorber medium are denoted by complex electric permittivity,ϵ as follows:

$$\epsilon(\lambda) = \epsilon^{'}(\lambda) + i\epsilon^{"}(\lambda) \tag{2.14}$$

The refractive index is defined as the square root of electric permittivity, therefore: [14].

$$n = \sqrt{\epsilon} = n + i\kappa \tag{2.15}$$

where κ represents the imaginary part of the refractive index. Lambert-Beer law is used to describe the behaviour of light when it passes through a medium which is shown below as follows: [14].

$$I(z) = I_0 \exp(-2k_z^{"}z) = I_0 exp(-\alpha z) \tag{2.16}$$

where α is the absorption coefficient, I_0 is the initial intensity at the surface, z is the path length and I(z) is the intensity of light in the medium. The absorption coefficient, α is a material property which is dependent of the wavelength of light. It is expressed as [29]:

$$\alpha = 2k_z^{"} = 2\frac{\kappa\omega}{c} = \frac{4\pi\kappa}{\lambda_0} \tag{2.17}$$

In order to measure the total absorptivity of a material at a certain wavelength, a parameter called penetration depth is used which is expressed as follows: [14]

$$\delta p = \frac{1}{\alpha} \tag{2.18}$$

2.4. Solar cell losses

Due to multiple factors which lead to losses, a solar cell is unable to utilize 100% of the incident light to convert it into usable energy. The theoretical efficiency for single junction solar cells is limited by the Shockley-Queisser (SQ) limit. The SQ limit considers a two-step approach, which include the losses due to the temperature of the solar cell being above 0K and spectral mismatch [29].

2.4.1. Spectral mismatch

The most crucial area of the solar cell is the absorber layer which is composed of semiconductor material such as silicon with bandgap energy, E_g. Useful work is only achieved when the energy of the photons is higher than the bandgap energy. The electrons are usually present in the bottom of the conduction band while holes usually lie on top of the valence band. Therefore, the excess energy given to the electrons and holes are released in the form of heat, which is known as thermalization loss. Meanwhile, the photons which have lower energy than that of the bandgap cannot generate electron hole pairs and hence also contribute to the losses. Shockley and Queisser defined a maximum efficiency which can be attained by solar cells after all the spectral mismatch losses which is defined as Shockley Queisser limit. The highest attainable efficiency is the product of the absorbed power (P_{abs}) with the useful power (P_{use}) [14]. The absorbed power is defined as the ratio of power absorbed by the solar cell to the total incident power. A fraction of the absorbed power is lost due to thermalization. Therefore, the remaining is the useful power, P_{use}. The equation for the absolute power as well as the useful power are given below as follows [29]:

$$P_{abs} = \frac{\int_0^{\lambda} G \frac{hc}{\lambda} \phi_{ph,\lambda} d\lambda}{\int_0^{\infty} \frac{hc}{\lambda} \phi_{ph,\lambda} d\lambda} \tag{2.19}$$

$$P_{use} = \frac{E_G \int_0^{\lambda} G \frac{hc}{\lambda} \phi_{ph,\lambda} d\lambda}{\int_0^{\lambda} G \frac{hc}{\lambda} \phi_{ph,\lambda} d\lambda} \tag{2.20}$$

The ultimate efficiency takes into account the solar cells at 0K while there exist further losses such as open-circuit voltage loss, non-zero recombination current density and fill factor losses. These are explained further in section 2.4.3 [29].

2.4.2. Optical losses

The optical losses do not constitute the Shockley Queisser limit despite it playing a significant role in determining the efficiency for solar cells.The optical properties usually dependent on the wavelength of the incident light and can be expressed through the complex refractive index, $n = n - i\kappa$.The interface between two media is described by the wavelength dependent reflectance and transmittance. Total efficiency of the solar cell is impacted by the reflections and transmittance experienced by the light when it passes through the absorber layer [29].

Another significant loss experienced by solar cells are the shading losses. Usually, solar panels have thin metal strips on the panel surface which serve as electrodes. This strip however blocks some of the light which would otherwise have entered the solar cell. Therefore, these strips overall decrease the active area where the light could have been absorbed into a solar cell and hence these are described as the shading losses. However, a reduction in the thickness of the metal strip also leads to a higher series resistance, hence an optimal tradeoff must be kept to ensure desirable efficiencies.

Another type of optical loss is parasitic absorption. Usually, the solar cells is made of multiple layers with the absorber layer being the only layer which helps to generate current. Usually, some of the light passing through the solar cell gets absorbed in other layers expect the absorber layer. This type of loss is referred to as the parasitic absorption loss [29].

2.4.3. Additional losses:

There are few other loss mechanisms that lead to loss of efficiency. They are as follows:

- Voltage drop due to increased series resistance which occurs as a result of the bulk resistance of the junction, the resistance of the electrodes and the contact resistance between the junction.
- Voltage drop due to leakage current which occurs due to shunts, for instance at the edges of the solar cell.
- Decrease in fill factor as a result of different recombination mechanisms in a non-ideal solar cell.

The overall summary of the losses across a solar cell is represented by figure 2.3 below:

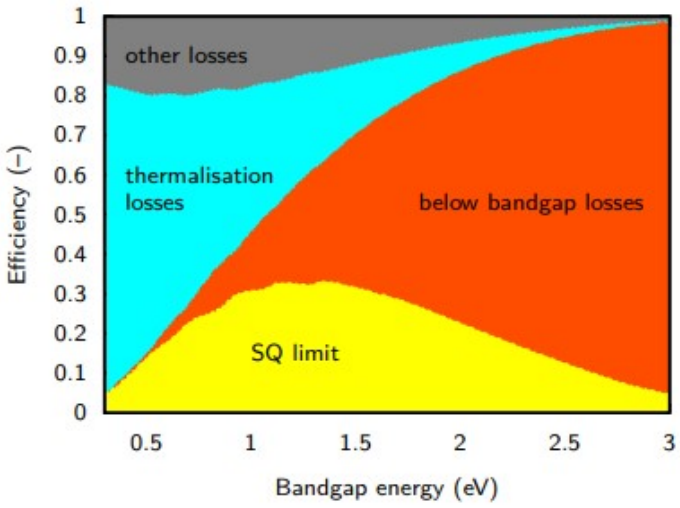

Figure 2.3: Different solar cell losses [29]

2.5. Strategies to Prevent Losses in Solar cells:

To reduce the spectral mismatch losses, optical losses and other additional losses, three design rules have been formulated:

2.5.1. Bandgap utilization

It is seen that the open-circuit voltage of the solar cell is always lower than the bandgap voltage. This loss is expressed by the bandgap utilization efficiency. Bandgap utilization aims to minimize this loss in order to make the solar cells more efficient. The dominant recombination mechanism limits the open-circuit voltage. The type of dominant recombination mechanism depends on the illumination conditions and type of semiconductor used in the solar cell [14].

2.5.2. Spectral utilization

Spectral utilization involves utilizing the energy of the incident length especially in the UV-Visible range in order to generate higher currents and therefore higher efficiencies. The materials which constitute the solar cells play a major role in determining the spectral utilization of the solar cell, hence the bandgap of the materials must be close to in order to ensure good spectral utilization [29].

2.5.3. Light Management

It is desirable to have all the incident light on a solar cell to be absorbed in the absorber layer. The Lambert-Beer law shows that the light intensity decreases exponentially as it travels through an absorptive medium. It can also be inferred that less light is absorbed from the front side where the light enters from compared to the backside. Therefore, an optically thick absorber layer is required to absorb all the incident light [29]. Amorphous silicon is a better absorber compared to crystalline silicon because of the direct bandgap nature and low bandgap energy required. This helps in realizing thin absorber layers in thin-film technologies [19]. It is important to reduce the other optical losses such as reflection, parasitic absorption, and shading losses by using light management techniques.Anti-reflective coatings can be used to reduce reflection losses.An inter-layer can be introduced with a refractive index n_1, which has a value in between the refractive index of air (n_0) and that of silicon (n_2). If no multiple reflections are considered, the reflectance can be minimized when the following condition is satisfied [29]:

$$n_1 = \sqrt{n_0 n_2} \tag{2.21}$$

Figure 2.4 shows how the total reflectance decreases significantly with the introduction of an anti-reflection coating with a refractive index in between the values of the other two layers [29].

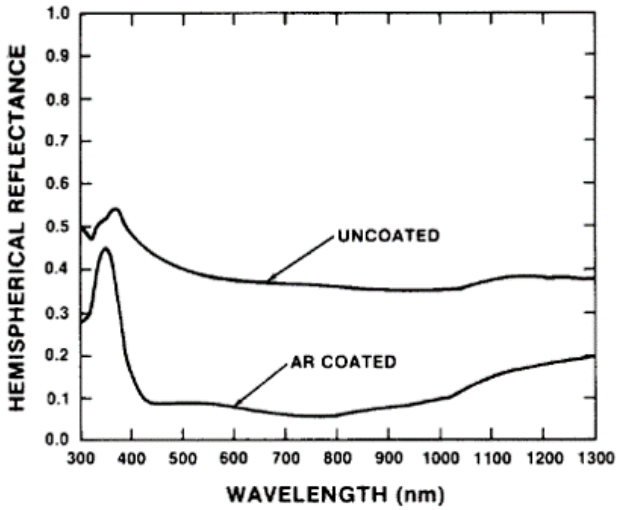

Figure 2.4: Reflectance measurement for a sample without and with double antireflection (AR) coating [30]

2.5.4. Texturing

Another approach to minimize losses could be the use of textured surfaces. This process ensures an increase in the optical path of light across the solar cell. As the incident light falls on the textured surface, the light gets reflected to other parts of the textured surface. This ensures that the light remains in the active region for a longer time which is essential to generate higher efficiencies.A Textured process is usually achieved by either wet or dry chemical etching [29]. The path of the incident light through a textured surface is illustrated below in figure 2.5 as follows:

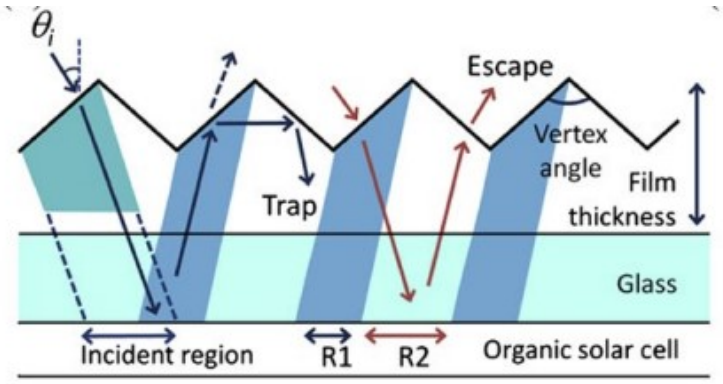

Figure 2.5: Path of incident light through the textured surface [31]

3

Literature Review

This chapter discusses the significance of the TCO layer in thin film photovoltaics as well as the current TCO used at HyET Solar. It also lays emphasis on the texturing process at HyET Solar as well as its importance in obtaining higher performances.Section 3.1 explains the importance of TCO especially in thin film solar cells.Section 3.2 discusses the different TCO layers used in thin film solar cells. Section 3.3 discusses the TCO characterization process implemented in this thesis to study the electrical as well as the structural properties of the TCO.Finally section 3.4 lays emphasis on the importance of texturing as well as the different types of textures used at HyET Solar.

3.1. Transparent Conductive Oxide(TCO)

To ensure rapid development of photovoltaics (PV), it is essential for the investment costs to be low which is one of the main factors which hinder the growth of PV technology. One way to ensure significant cost reduction is the adoption of thin film solar cells which are based on hydrogenated amorphous (a-Si:H) or nanocrystalline (nc-Si:H) silicon and their alloys [32]. Transparent conductive oxides(TCOs) are an essential part of these cells which are used as a front electrode and also as a back side reflector. If the TCO is applied on the front side of the solar cell, it is essential for it to have a high transparency within the solar cell spectrum while also possessing a high electrical conductivity. Other than these two parameters, it is also essential for the TCO to have strong scattering properties to allow sunlight into the silicon absorber layer and it should also possess ideal physio-chemical properties to ensure the growth of silicon [33].

Different TCOs commonly used in solar cells include undoped and fluorine-doped tin oxide (SnO_2 and $SnO_2 : F$), indium oxide (In_2O_3), indium tin oxide (ITO), and undoped and doped zinc oxide (ZnO).TCOs are deposited on the solar cells through different methods such as chemical vapor deposition (CVD), sputtering, sol–gel process, and spray pyrolysis (SP).Among them, Sputtering and evaporation processes are expensive processes hence are not used in industrial applications. On the other hand, chemical vapor deposition and spray pyrolysis are often used for large scale production of the TCO due to its low cost and easy operation [34].

3.2. Types of Transparent Conductive Oxide(TCOs)

3.2.1. Indium doped Tin Oxide(ITO)

Indium tin oxide or ITO is a n-type semiconductor with a wide band gap of around 3.5–4.3 eV [35]. It ensures high transmission especially in the visible range, and it also processes great electrical conductivity in the range of 2500–5000 $\Omega^{-1}cm^{-1}$ [35]. Therefore, due to these optimal properties, ITO is used in several applications which includes solar cells, heat-reflecting mirrors, gas sensors and anti-reflection coatings [35]. ITO films also demonstrate great efficiencies for hole generation for organic materials, thereby finding its application as an anodic contact in the organic light-emitting diodes (OLEDs) [36]. ITO films are deposited through various techniques such as magnetron sputtering [37, 38] chemical vapor deposition (CVD) [39], spray pyrolysis [40] and pulsed laser deposition (PLD) [41]. Among all

these techniques, PLD is the most preferred as it yields highly crystallized and smooth deposition [41].

Some disadvantages which limit the use of ITO is its high production cost as indium is a rare metal and is in shortage currently across the world. Hence alternate films such as aluminium doped zinc oxide (AZO) and fluorine doped tin oxide(FTO) have sprung up in recent years which demonstrate similar properties to that of ITO while also maintaining a lower production cost. [42, 43].

3.2.2. Aluminium Doped Zinc Oxide(AZO)

Aluminium doped zinc oxide or AZO is another type of TCO which is a great alternative to the ITO films. It has gained popularity in recent years due to its great electrical and optical properties which are very similar to that of ITO. Additionally, it is also cost effective and offers great stability in hydrogen atmosphere as well. Thin ZnO films usually is doped with aluminium which helps to enhance the electrical conductivity, while also ensuring a high mobility and charge carrier density [44].

The AZO also demonstrates great transmittance of around 90% especially in the visible region. It also processes great infrared reflectivity and high UV conductance. Although AZO films have several advantages, they are known to be unstable especially in acidic or alkaline environments which limits its application in industries [45].

3.2.3. Tin oxide(TO) and Fluorine Doped Tin Oxide(FTO)

Tin dioxide (TO) films are also great alternatives to the ITO films as the TCO for solar cells. They exhibit great advantages, such as low cost, high abundance of raw materials and nontoxic in nature.SnO_2 films also demonstrate high transmittance in the visible region, has high near-infrared light reflectivity, and processes great electrical properties.They also have a better chemical and mechanical stability compared to ITO films.However, its electrical conductivity is much less compared to the other TCOs and it has eventually been replaced by fluorine doped tin oxides, where fluorine doping ensures great electrical properties for the TCO films [46].

Florine-doped tin oxide (FTO) thin films are widely popular for use as TCOs for solar cells due to their high electric conduction and great optical transparency in the visible region. Therefore, they find their use in several applications such as thin-film solar cells, sensors, organic light emitting diodes, transparent heaters, and architectural glass [47, 48, 49]. FTO also demonstrates several further advantages as it processes a wide energy bandgap, lower production cost, high transparency, and great mechanical and thermal stability [47, 50, 51]. However, its main disadvantage is that is its electrical conductivity is lower than AZO and ITO. However, the electrical conductivity of FTO remains lower than that of indium tin-doped indium oxide (ITO) [52]. Therefore, the oxygen atoms in tin oxide is replaced by fluorine atoms which help to improve the electrical properties of the FTO [51].

FTO thin films are deposited through various methods, such as atmosphere pressure chemical vapor deposition (APCVD) [49], sputtering [50], sol-gel [51, 53], and spray pyrolysis deposition (SPD) [47, 54]. Among the various techniques, atmospheric pressure chemical vapor deposition is the most favourable due to its high scalability, low cost and it is simple to implement. Due to its great optical and electrical properties and lower production costs, FTO is used as the TCO layer for the HyET Solar modules and hence this will be the topic of attention for this thesis as well.

Advanced process chemical vapour deposition (APCVD) process is used for the FTO deposition at HyET Solar. In this process, the aluminium foil is fed into the APCVD where it is heated upto 500°C. There are two injectors present which are responsible for depositing the TCO layer onto the foil. The injectors are responsible for depositing the gases $SnCl_4$, H_2O with small proportions of methanol and HF with nitrogen gas as the carrier. The schematic representation of the APCVD process at HyET Solar is shown below in figure 3.1.

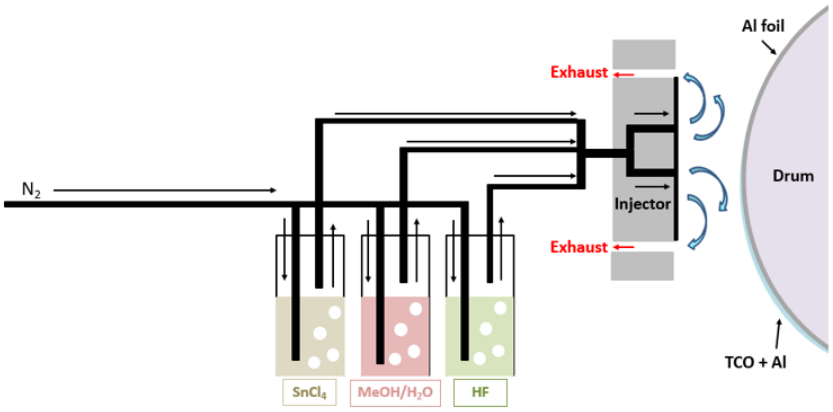

Figure 3.1: Schematic representation of the APCVD process used at HYET Solar for FTO deposition

3.3. TCO characterization techniques

3.3.1. Rsq measurement

Sheet resistance is an electrical parameter which helps in the electrical characterization of thin film or semiconducting materials. It is defined as the lateral resistance exhibited by a thin film or semiconductor square.The equation for the calculation of the sheet resistance is given below as follows:

$$R_sq = \rho/t \tag{3.1}$$

where R_{sq} is the sheet resistance in Ω square, ρ is the resistivity in Ω cm, and t is the thickness in cm [24].

Typically, the sheet resistance of the TCO is measured by the four point probe method [55]. This method, however, is not reliable for measuring the sheet resistance of the TCO deposited on a metallic substrate such as aluminium. Therefore,in HyET, the sheet resistance is measured using a special tool in the company.A resistive thin oxide inter layer is present between the aluminium substrate and the TCO in order to ensure a partial flow of current through the layers.This situation is sketched in figures 3.2a and 3.2b for two different ratios of TCO sheet resistance and inter layer resistance. In figure 3.2a, the flow of current is observed to be higher on the TCO layer as the resistance of TCO is much less than the resistance of the oxide layer while in figure 3.2b, the flow of current is much higher on the aluminium as the resistance of the TCO is higher than the resistance of the oxide layer [24].

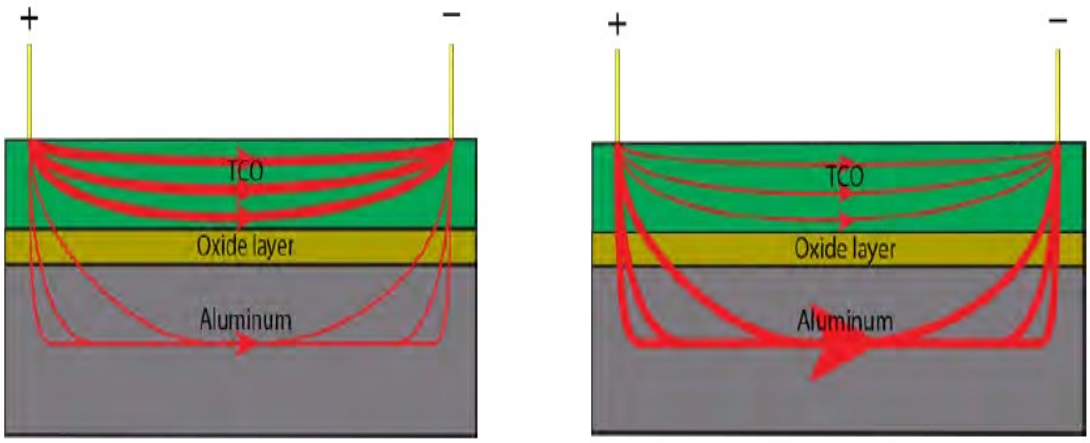

(a) R_{TCO} is lower than R_{oxide} [24]

(b) R_{TCO} is higher than R_{oxide} [24]

Figure 3.2: Flow of current through TCO+Al for the different ratios of TCO and the oxide layer [24]

The values of the resistances are determined by measuring the potential across the different areas of

the sample (1).The setup consists of voltage and current probes which are attached in grooves(2). The tool helps in measuring the sheet resistance locally in different areas which makes it easier to study the variations across the different areas of the modules. The sheet resistance tool setup is shown below in figure 3.3. The sample is placed flat on a cylindrical surface (3).The probes are contacted with the sample with the help of an adjustable arm which is controlled with the help of a lever.A 100-mA current is then passed with help of a Keithley source meter (4) which measures the potential across the voltage and records the sheet resistance measurement with the help of a NI DAQ 6211 device (5) which is then sent to the PC [24].

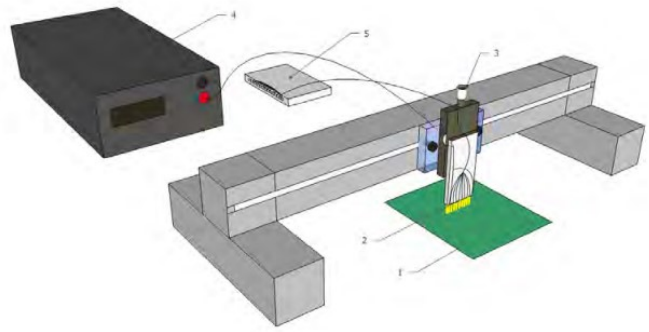

Figure 3.3: Schematic representation of the sheet resistance tool at HyET Solar [24]

3.3.2. TCO Leak Test

The TCO leak test is an indigenous test at HyET which is used to check how resistive the TCO is against the etch bath. It gives a good impression of the TCO deposition by identifying the pinholes/cracks in the TCO layers which can be exposed during the etching process. The leak test is conducted by taping the TCO sample to a board which is etch resistant. The taping is done in such a way that the only the TCO layer is exposed to the etch bath while the aluminium is completely stuck to the board. Ideally, HyET desires to achieve TCO leak times of at least 1 min which indicates an acceptable TCO morphological quality. Before performing the leak test, each sample was cut into two parts where one part was used for the TCO leak test while the other sample was taken to Delft for the structural characterization tests of the TCO (SEM, confocal microscopy(CM)).

3.3.3. Scanning Electron Microscopy(SEM)

SEM stands for scanning electron microscopy. It makes use of an electron beam instead of light which ensures accurate images of samples upto the nanometer scale [56].The electron gun at the top of the microscope is responsible for producing the electrons beam. The beam passes vertically through the microscope in vacuum.The beam passes through the electromagnetic fields which is then passed onto the sample with the help of lens. When the electron beam hits the sample, some electrons and X-rays are reflected back which is then converted into a signal which then projects the final image on the computer [57]. The schematic representation of an SEM is given below in figure 3.4. For SEM imaging, Regulus 8230 was used from TU Delft due to its high resolution upto 0.7 nm which ensured highly accurate images.The microscope employs a novel cold-field-emission(CFE) gun which ensures high resolution images at low acceleration voltages. This CFE gun makes it possible to magnify an image by a factor of upto 2 million [58].

In this thesis, the microscope is used to observe the quality of the TCO in which the cracks, pinholes, and uniformity of the TCO is observed. Also, cross sectional SEM has been used to determine the actual thickness of the TCO. As the TCO was deposited on aluminium substrate, low acceleration voltage was used as high voltages led to blurred and poor-quality images. The schematic representation of the SEM Hitachi Regulus 8230 used for this thesis is depicted below in figure 3.5.

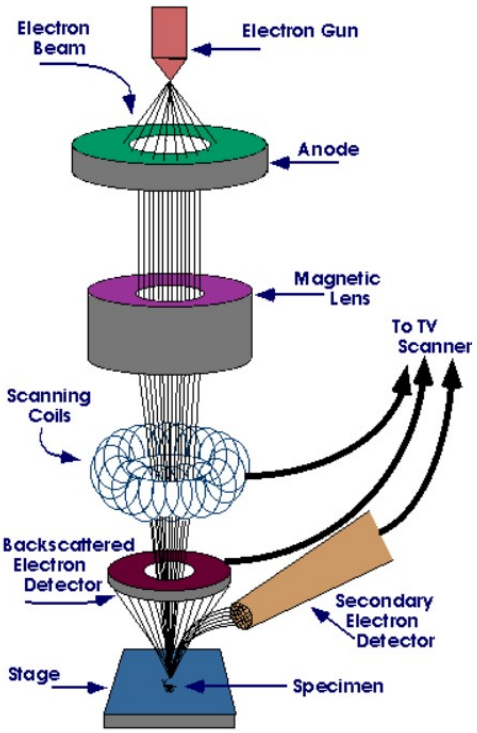

Figure 3.4: Schematic representation of Scanning electron microscope(SEM) [57]

Figure 3.5: Schematic representation of the SEM Hitachi Regulus S8230 [59]

3.3.4. Confocal Microscopy (CM)

Confocal microscopy (CM) is an optical imaging technique which helps to increase the optical resolution and contrast of a micrograph through the use of a spatial pinhole which blocks out of focus light to ensure accurate images. As it captures multiple two-dimensional images of the sample at different depths, it hence also ensures that three-dimensional representation of the sample can also be observed. Hence this microscope finds its applications in several industries most notably the life sciences, material science and the semiconductor industry.

Unlike a normal microscope where the light travels through the sample and penetrates as far as possible on the sample, the confocal microscopy only focuses a smaller beam of light at the sample with a particular depth at a time which ensures highly controlled depth of field thereby ensuring accurate and high-resolution images [60].The Light from a laser source is passed to a dichromatic mirror which reflects the light to the objective lens which then focuses the beam onto the sample. The scanning mirrors help in focusing the beam over the sample which then builds the image. A pinhole is placed

which prevents the out of focus light from forming the image [61].Figure 3.6 depicts a schematic of the confocal microscopy.

The Keyence VK-X Series 3D Laser Scanning Confocal Microscope helps in providing a non-contact, roughness, and film thickness data for any material. The microscope has a lateral resolution of 120 nm using the 408 nm Violet laser light. The 16-bit photomultiplier helps to scan the surface which then receives the reflected laser light. The instrument provides a highly accurate 3D measurement data over any material shape up to an angle of 88 Degrees [62].

In this thesis, the confocal microscopy is used to study the roughness of the TCO as well as the aluminium foil.The schematic representation of the Keyence confocal microscopy used for this thesis is depicted below in figure 3.7.The confocal microscopy gives information regarding the different roughness parameters such as S_a, S_z and S_{pc}.S_a is defined as the arithmetic mean height which compares the difference in height of each point to the arithmetic mean of the surface which helps to evaluate the roughness of the surface.$S_z$is the maximum height which is the sum of the largest peak height value and the largest trough depth value within a particular area. Lastly, S_{pc} is the maximum height peak which indicates the height of the maximum peak within a particular area. It is desired to keep these roughness parameters as low as possible to ensure a homogeneous deposition of the different layers [63].

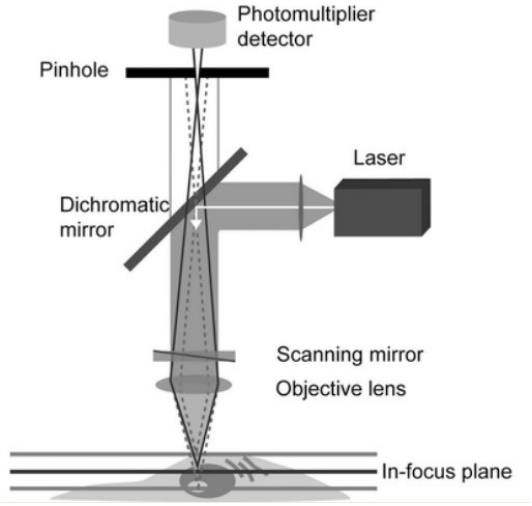

Figure 3.6: Schematic representation of the confocal Microscope(CM) [61]

Figure 3.7: Schematic representation of Keyence confocal Microscopy Setup used at TU Delft [64]

3.4. Aluminium Texturing Process

Bare aluminium foil is used as the substrate at HyET solar in which all the deposition processes are done. It is created by rolling highly pure and thin rolled base foil into an even thinner gauge [65]. Usually, the amount of pure aluminium in the aluminium foil ranges from 92-99%. To improve the mechanical properties of the aluminium foil, it is usually doped with different elements such as manganese, copper, iron, silicon etc [66]. It is important that the aluminium foil is as clean as possible without any impurities such as dirt or grease which is essential to ensure a homogeneous deposition of the different layers. Before, the deposition process, the aluminium foil is subject to the texturing process [67].There are three different kinds of texturing done at HyET solar- Factory Baseline (FB), FLAM01 and FLAM02.The importance of texturing is already highlighted in section 2.5.4 in chapter 2.

The factory baseline and FLAM01 processes are usually performed on a 110 microns thick aluminium foil while the FLAM02 process is done on a 150 microns thick aluminium foil due to its high etch rate thereby providing a higher stability window which ensures greater mechanical stability in the subsequent manufacturing steps [67].

The surface of the bare aluminium foil is not uniform and does have some roughness. The SEM image for bare aluminium as well as the topography for the bare aluminium taken via the confocal microscope is highlighted below in figures 3.8 and 3.9 respectively.

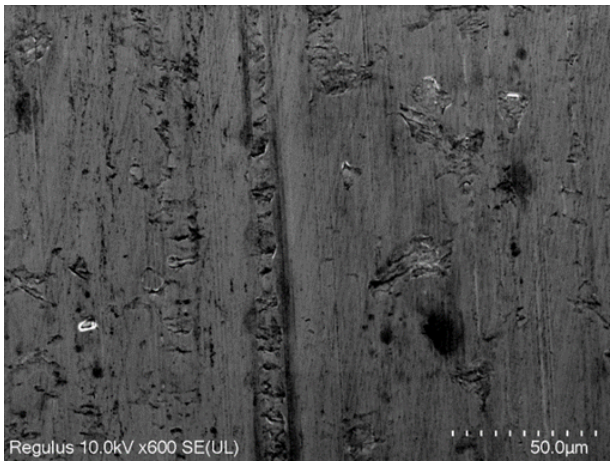

Figure 3.8: SEM Image for Bare aluminium foil used at HyET Solar

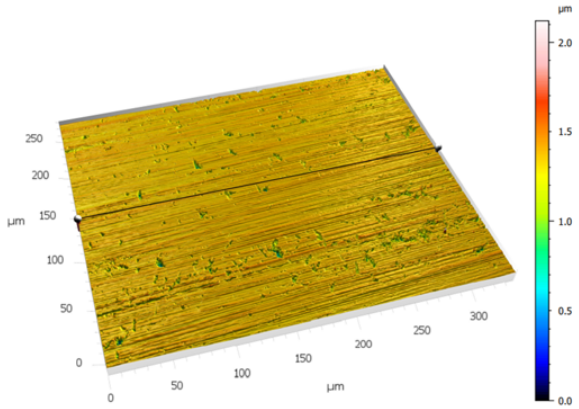

Figure 3.9: Topography of the surface roughness of bare aluminium foil used at HyET Solar

The bare aluminium exhibits high spectral reflectance of around 69% and low diffuse reflectance of around 15.6% across the wavelength range 200-2000 nm. Figure 3.10 shows the reflectance mea-

surements of bare aluminium foil. In order to reduce the spectral reflectance and increase its diffused reflectance for efficient light scattering, texturing is carried out on the aluminium foil using the wet chemical etching process.These textures are formed because of aluminium etching with the help of the NaOH etchant [67].The different types of texturing done at HyET solar is further explained in the sections below.

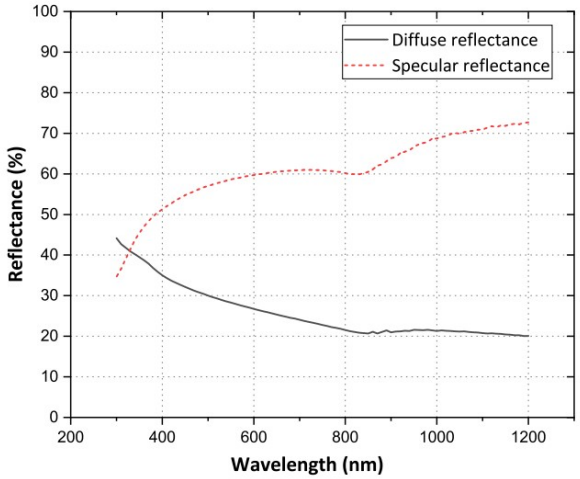

Figure 3.10: Spectral and diffused reflectance measurement for bare aluminium foil [67]

3.4.1. Factory Baseline (FB)

The factory baseline texturing (FB) is currently the baseline texturing process which is implemented at HyET. Wet chemical etching process with NaOH etchant is used for this texturing process. The temperature of the etchant is kept at a temperature of 35 degrees and the time for texturing is kept as 3.5 minutes. In order to prevent aluminium oxide precipitants from forming on the aluminium surface, chelating agents such sodium gluconate (1.8g/L), sodium nitrate (6g/L), and polyethylene glycol 400 (PEG-400) (0.4g/L) are added to the etch bath. Upon completion of the texturing process, the foil is cleaned with warm water to stop the etching reaction. It is then dipped in in 5 w/w% phosphoric acid solution in order to neutralize the base. It also helps in the removal of the precipitants which will be discussed further in chapter 5.The size of the textured craters of the foil from FB texturing is significantly less compared to the other two texturing processes. This process also acts as the baseline pre-treatment process in order to remove the oil, grease, dirt etch from the aluminium foil before the deposition processes [67].Figure 3.11 shows a SEM image of the factory baseline textured sample.

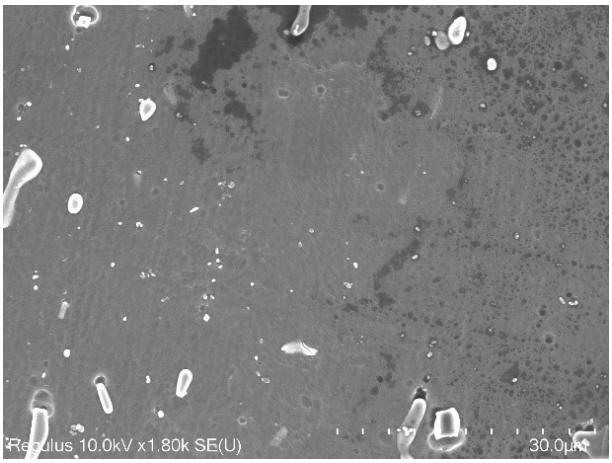

Figure 3.11: Factory Baseline(FB) texture

3.4.2. FLAM01 Texture

Similar to the factory baseline(FB) texturing, the FLAM01 texturing process is done using the wet chemical etching method at a temperature of 50 degrees and a time period of 1.8 minutes. The concentration of NaOH is 60g/L with sodium gluconate (13.2 g/L) and PEG-400 (2g/L) used as the chelating agents. The rest of the cleaning process after the FLAM01 texturing is the same as the factory baseline. Unlike the factory baseline texturing, the size and the number of craters are higher in FLAM01 texturing hence samples etched under this process will have should have better light trapping[67]. Figure 3.12 shows a SEM image of the FLAM01 textured sample.

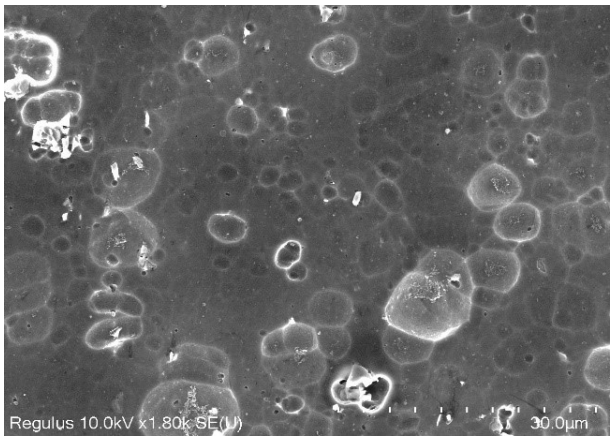

Figure 3.12: FLAM01 Texture

3.4.3. FLAM02 Texture

Unlike the previous two texturing processes which uses 110 microns thick Al foil, the FLAM02 texture is performed on 150 microns thick Al foil. The FLAM02 texturing recipe is obtained by further optimizing the FLAM01 parameters. The concentration of NaOH is 60 g/L at a temperature of 60 degrees and a time of 2.5 minutes.The FLAM02 texturing craters are much larger and are much more prevalent compared to the other two texturing counterparts and hence it can ensure much better light trapping compared to its other texturing counterparts [67]. Figure 3.13 highlights the FLAM02 texture on the aluminium foil.

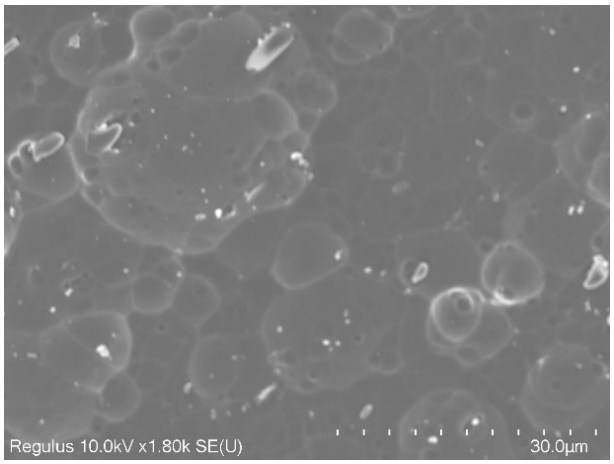

Figure 3.13: FLAM02 Texture

4

TCO Characterization

This chapter discusses the TCO thickness variations as well as the characterization procedure implemented in order to quantify the TCO at HyET.Section 4.1 explains the background and the motivation behind the implementation of the TCO characterization process.Section 4.2 discusses the experiments as well as the characterization process in detail.Section 4.3 discusses the observations as well as the results deduced from the TCO thickness variation experiment. Finally section 4.4 discusses the conclusions obtained through these set of experiments.

4.1. Background and Motivation

Earlier, the production at HyET Solar aimed towards the production of single junction modules. In recent years, the company has shifted its focus towards the production of tandem modules as they offer a better performance. Since the TCO settings were mainly used for production of single cell modules, it was essential to re-optimize the TCO for tandem modules. TCOs are transparent conductive oxide thin film layers which is often used as the front layer in thin film solar cells [68]. An optimal TCO is expected to have a resistivity lower than 10^{-3} Ω cm and a transmittance greater than 80% especially in the visible region. Therefore, to achieve this, it is essential that the TCO layer possesses bandgap of at least 3 eV and a charge carrier density of around $2 - 3 \times 10^{20}$ cm−3 [69, 70]. As explained in chapter 3, the TCO deposition at HyET Solar occurs through the atomospheric pressure chemical vapour deposition (APCVD) process. In this process, the aluminium foil is fed into the APCVD chamber where the Al oil is heated to 500°C. Afterwards, the TCO is deposited onto the Al foil with the help of two injectors present in the APCVD machine. The injectors help in delivering the gases $SnCl_4$, H_2O, methanol(MeOH) and hydrogen fluoride (HF) to the deposition chamber which then deposits the TCO on the aluminium foil.The TCO used in HyET solar is fluorine-based tin oxide (FTO) as it satisfies all the desired characteristics which a TCO needs to have, and it is also highly scalable due to its low production cost. In 2021, a new Al roll was purchased from the supplier which had an improved morphology compared to the previous batches.It was necessary to optimize the FTO thickness for this new Al roll so that it can be used in future production runs.Previously, the FTO characterization at HyET was limited to online diagnostics which unfortunately was not enough to quantify the TCO. Therefore, it was important to lay down an efficient characterization approach for the FTO which will give HyET useful information regarding the FTO such as its morphology and electrical characteristics which will make it easier to judge whether the FTO meets the desired standards or not. This procedure will also make it easier to plan and optimize the FTO in the future. The TCO characterization procedure implemented during this thesis is depicted in figure 4.1.The importance of the characterizations and the desired results from them are shown below in table .Additionally, the TCO characterization was compared for both the 2020 and 2021 Al foils to observe if the quality of the aluminium foil impacted the performance of the HyET Solar modules.

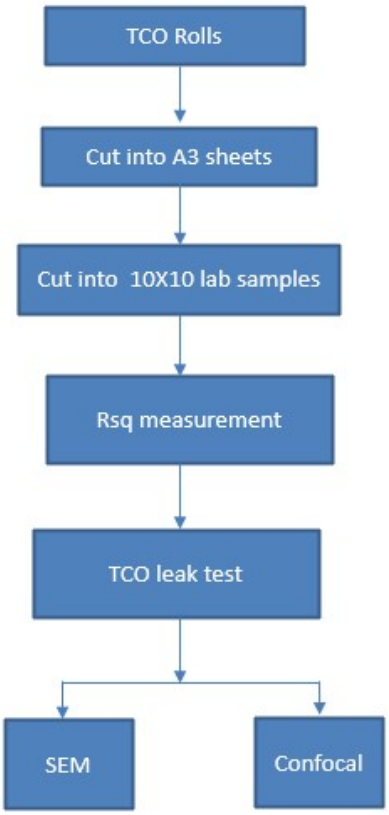

Figure 4.1: Procedure for TCO characterization

Characterization	Type of characterization	Desired Result
Sheet resistance	Electrical	10 Ω sq. sheet resistance
TCO Leak test	Structural	Leak time of 1 min
Scanning Electron microscopy(SEM)	Structural	Low cracks/pinholes across TCO surface
Confocal microscopy(CM)	Structural	Low roughness parameters

Table 4.1: TCO characterization measurements implemented in this thesis

4.2. Experimental Procedure

For the aluminium roll introduced in November 2021, the TCO thicknesses were varied between 650 nm to 800 nm. These variations in thicknesses were performed for both the untreated as well as the pre-treated rolls. Untreated roll is the roll from the supplier which is used as it is and is not subject to any cleaning procedure whereas the pre-treated roll is subject to the factory baseline texturing (FB) to remove oil/grease and other surface impurities from the aluminium roll. The main reason behind performing the experiment is to observe the effect of the texturing process on the TCO quality, and ultimately the device performance.The variations of the TCO thicknesses for both the untreated as well as the pre-treated roll is highlighted below in table. Settings 1.1-1.5 depict the untreated Al roll while settings 2.1-2.4 depict the pre-treated roll. The TCO thicknesses were varied according to the web speed in the APCVD chamber and variations determined by the inline diagnostics is shown below in figure 4.2.

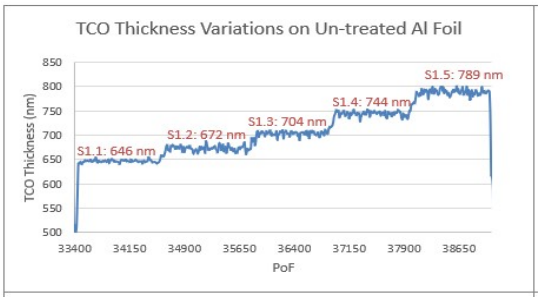

(a) TCO Thickness variations on untreated Al roll

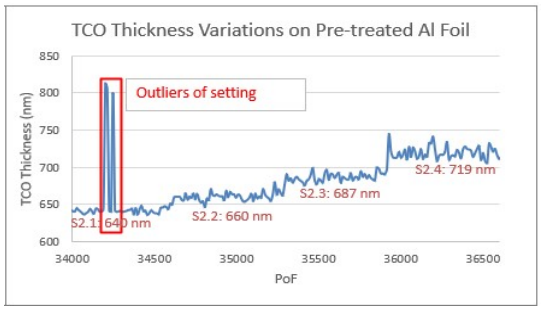

(b) TCO Thickness variations on pre-treated Al roll

Figure 4.2: TCO thickness variations of untreated and pre-treated roll from inline diagnostics at HyET

Setting	Type of Al foil	TCO Thickness(nm)
1.1	untreated	650
1.2	untreated	675
1.3	untreated	705
1.4	untreated	745
1.5	untreated	790
2.1	pre-treated	647
2.2	pre-treated	660
2.3	pre-treated	687
2.4	pre-treated	719

Table 4.2: TCO thicknesses for pre-treated and untreated Al roll

The aluminium rolls were cut into A3 sheets for each of the settings for both the untreated as well as the pre-treated rolls. Afterwards, each A3 sheet was cut into 4 $10 \times 10cm^2$ lab samples per setting using the special 10×10 lab sample cutter at HyET. The samples were further divided with respect to their positions in the A3 sheet as com 115 and com 255. COM 115 indicates that the centre of the sample is at a distance of 115 mm from the edge of the foil while COM 255 indicates that its centre is around a distance of 255 mm from the same edge of the foil. Therefore, two samples of COM 115 and COM 255 were taken for each setting. The variations of the TCO thicknesses across the COMs is shown below in figure 4.3.

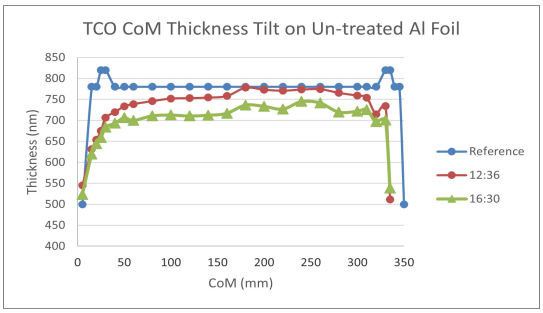

(a) Variations of the centre of module(COM) across the untreated Al Roll

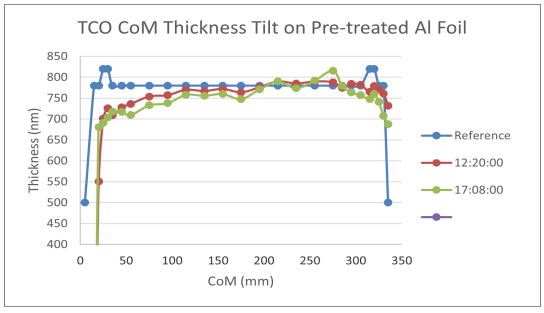

(b) Variations of the centre of module(COM) across the pre-treated Al Roll

Figure 4.3: Variations of the centre of module(COM) across the untreated and pre-treated Al Roll determined by the inline diagnostics at HyET

The first measurement done was the sheet resistance measurement which was done with the help of the sheet resistance tool at HyET, as explained earlier in section 3.3.1.Afterwards, the sample was cut into two parts of which the first part is used for the TCO leak test while the second part is then taken to TU Delft where the structural characterizations of SEM and confocal microscopy takes place.

4.3. Observations and Results

This section discusses the different measurements taken as well as the observations and results which can be deduced from these measurements.

4.3.1. Sheet Resistance Measurement

After the lab samples are made for the TCO on aluminium substrate, the first measurement done is the sheet resistance measurement. Ideally, as explained in section 3.3.1, it is desired for the sheet resistance to be around 10 Ω square. The sheet resistance measurements for both the untreated as well as the pre-treated aluminium foils on TCO is given below in figure 4.4. Additionally, the sheet resistance measurement has also been taken for the TCO deposited on previous Al batch to observe if the TCOs deposited in the new roll have lower sheet resistances.

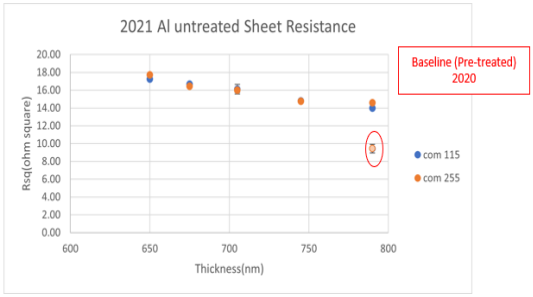

(a) Sheet Resistance measurement for untreated Al Roll

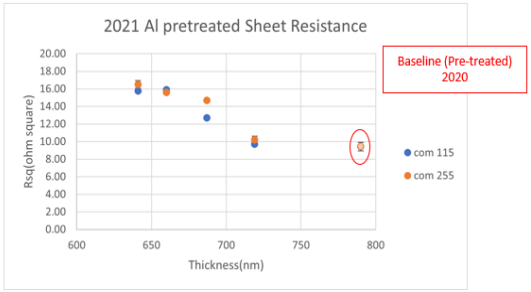

(b) Sheet Resistance measurement for pre-treated Al Roll

Figure 4.4: Sheet Resistance measurement for both untreated and pre-treated Al roll

From the graphs shown in figure 4.4, it can be observed that the sheet resistance appears to decrease with the increase in the TCO thickness for both the untreated as well as the pre-treated rolls. Also, the pre-treated aluminium samples appear to have a lower sheet resistance compared to the untreated aluminium samples which could be due to the absence of oil/grease on the aluminium samples which are removed through the pre-treatment process. Additionally, it can be observed that the untreated foil of thickness 790 nm(S1.5) and pre-treated foil of thickness 720 nm(S2.4) appear to give the lowest sheet resistances of 14 Ω sq and 10 Ω sq respectively.

4.3.2. TCO Leak Test

After the measurement of the sheet resistance of the samples which gave a good indication regarding the resistance of the TCO layers, the samples were then subject to the TCO leak test which has been explained previously in 3.3.2. Ideally, it is desired to have TCO leak times of at least 1 min which ensures that the TCO quality is in spec, and has sufficiently lower concentration of cracks and pinholes. The TCO leak test results for both the pre-treated as well as the untreated samples are depicted below in figure 4.5.

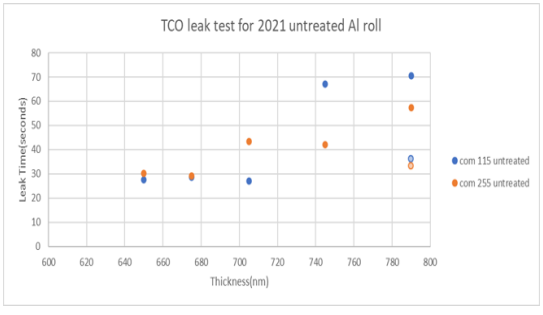

(a) TCO leak test for untreated Al Roll

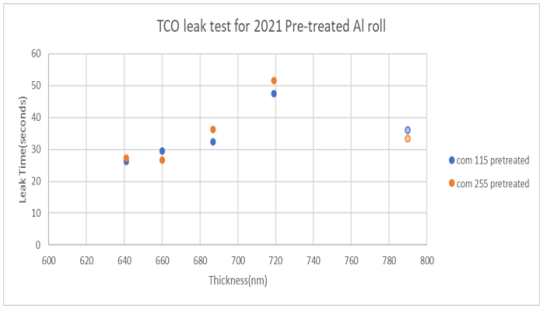

(b) TCO leak test for pre-treated Al Roll

Figure 4.5: TCO leak test measurements for both untreated and pre-treated Al roll

From the TCO leak test results shown above in figure 4.5, it can be observed that the untreated sam-

ples have higher leak times compared to the pre-treated samples which could indicate that more pin-holes/cracks are forming on the aluminium surface during the pre-treatment process. Also, it can be observed that the TCO leak time appears to increase with the increase in thickness of the TCO layer for both the pre-treated as well as the untreated samples. Lastly, the COM 255 samples also appear to outperform the COM 115 samples in most of the cases which could also be due to their higher thickness as observed in figure 4.3. Overall, it was observed that the untreated foil of thickness 790 nm (S1.5) and pre-treated foil of thickness 720 nm (S2.4) appear to give the best leak times of 70 sec and 50 sec respectively.

4.3.3. Confocal Microscopy

Each sample was cut into 1X1 cm^2 area before the sample was placed in the Keyence 3D confocal microscope to discover the surface roughness of the different TCO layers present on the aluminium substrate. The confocal microscopy measurements highlighting the roughness parameters of S_a, S_z and S_{pc} for both the pre-treated and untreated Al samples for each of the TCO thickness settings is highlighted below in figure 4.6 as follows:

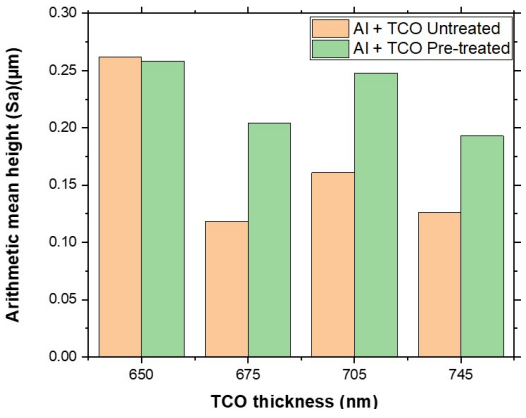

(a) Aritmetic Mean height(S_a) measurements

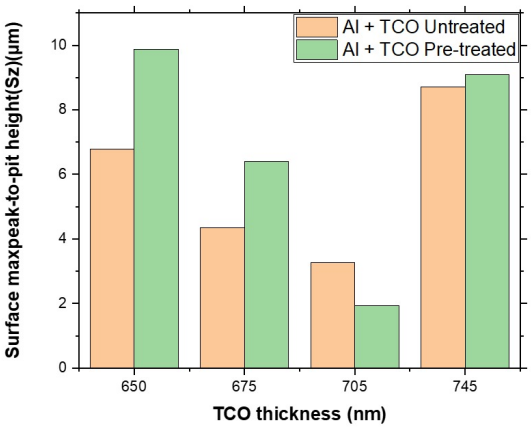

(b) Surface max peak to pit ratio(S_z) measurements

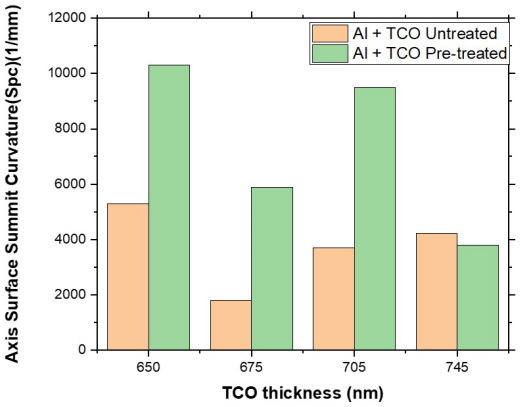

(c) Axis surface summit curvature(S_{pc}) measurements

Figure 4.6: Surface roughness parameters for both untreated as well as pre-treated Al Rolls [71]

(a) 3D confocal microscope image for untreated Al Roll

(b) 3D confocal microscope image for pre-treated Al Roll

Figure 4.7: 3D confocal microscope images for untreated and pre-treated Al Roll [71]

From figure 4.7, it can be observed that the pre-treated samples appear to have higher surface irregularities(cracks/pinholes) compared to the untreated samples. Through figure 4.6, it can be also observed that the surface roughness S_a, S_z and S_{pc} parameters are higher for the pre-treated samples.

4.3.4. Scanning Electron Microscopy(SEM)

After the confocal microscopy measurements, the samples were once again cut into 1X1 cm^2 areas and these were subject to the SEM characterization to determine the quality of the TCO (observe the uniformity, presence of cracks/pinholes). Figures 4.8 and 4.9 highlight the SEM images for both the untreated as well as the pre-treated samples respectively.

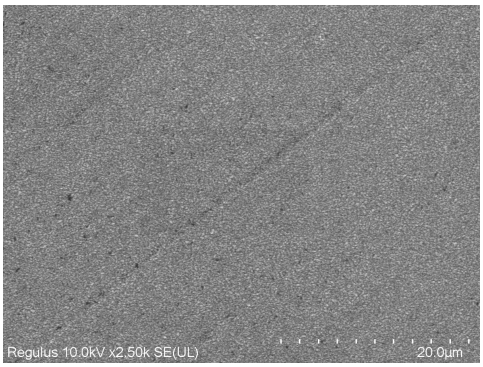

(a)

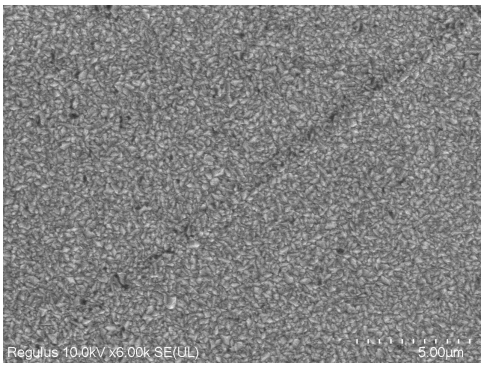

(b)

Figure 4.8: SEM images for untreated Al samples at (a)20 microns and (b)5 microns magnification

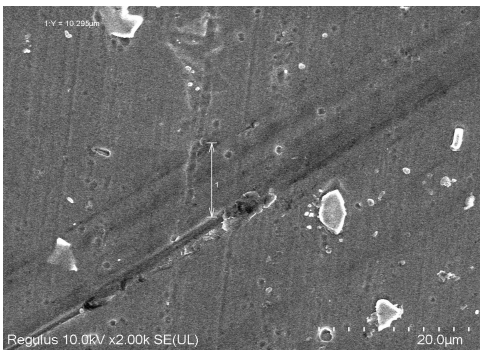

(a)

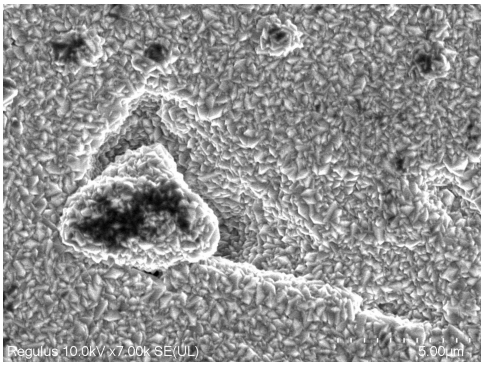

(b)

Figure 4.9: SEM images for pre-treated Al samples at (a)20 microns and (b)5 microns magnification

From the SEM images, the pre-treated samples appear to have more surface irregularities compared to the untreated aluminium samples. Also, there appears to be presence of small irregular particles

across the surface of the pre-treated samples. Usually, the Al foil at HyET is doped with different metals such as iron, manganese, silicon etc in order to boost the mechanical properties of the Al foil. This step is necessary as it ensures stability of the aluminium foil at higher temperatures which are required for the TCO as well as the silicon depositions. These irregularities are referred to as the precipitants in this thesis and this will be discussed and addressed in detail in chapter 5.Lastly, the presence of milling tracks is observed for both the samples, but it is more prevalent in the pre-treated samples.

Afterwards, cross-sectional SEM analysis was done for the samples to determine the actual thickness of the TCO layer in each sample. As this was only done to ensure the actual thickness was similar to the optical thickness of the TCO determined by the APCVD diagnostics, the results are presented for only the untreated aluminium roll. The cross-sectional SEM analysis is highlighted below in figure 4.10.

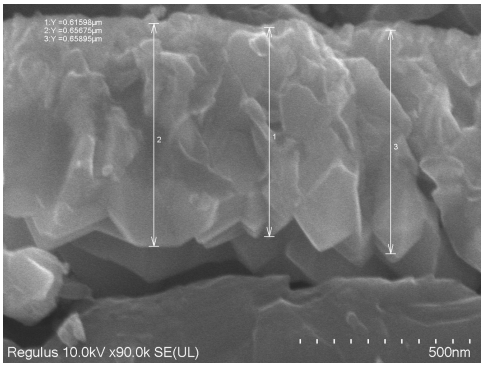

(a) Cross sectional SEM analysis for TCO setting S1.1:650nm

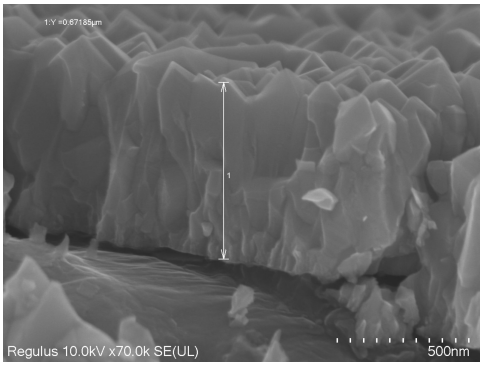

(b) Cross sectional SEM analysis for TCO setting S1.2:675nm

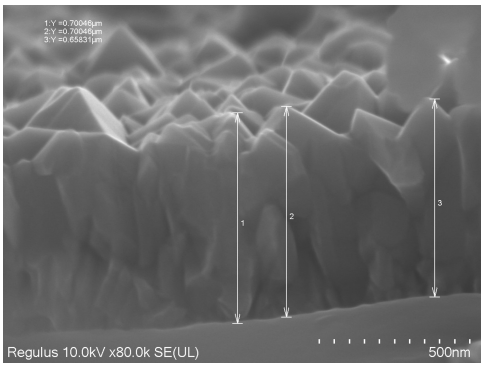

(c) Cross sectional SEM analysis for TCO setting S1.3:705nm

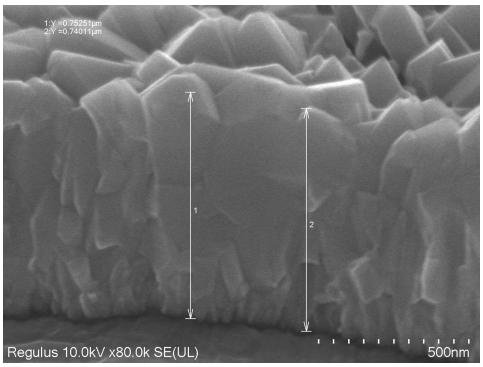

(d) Cross sectional SEM analysis for TCO setting S1.4:745nm

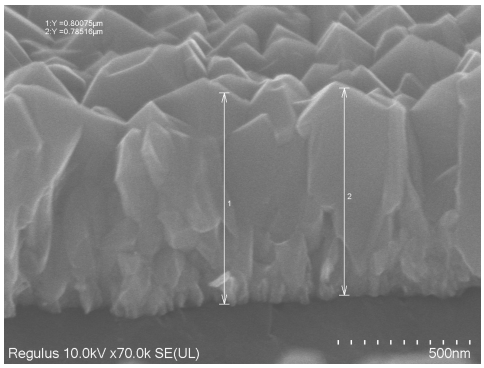

(e) Cross sectional SEM analysis for TCO setting S1.5:790nm

Figure 4.10: Cross sectional SEM analysis for untreated Al Roll samples [71]

From the cross-sectional SEM images, it can be observed that the actual thickness appears to be similar to the optical thickness measured by the APCVD diagnostics. Through this, it can be confirmed

that optical measurement by the APCVD diagnostics tool at HyET is accurate.

4.4. Conclusions

Overall, through this set of experiments, an efficient and reliable approach was set for characterization of the TCO at HyET Solar. Overall, different types of TCO characterization tests were carried out which helped to better understand the characteristics of the TCO especially with regards to their electrical and structural properties. Optical properties unfortunately could not be explored as the aluminium substrate as well as the PEN substrate could not provide reliable transmission measurements. Firstly, the TCO test carried out was the sheet resistance measurement during which it was observed that the pre-treated samples had lower sheet resistances compared to the untreated samples. It was also observed that the TCO sheet resistance appeared to decrease with the increase in the thickness of the TCO. The sheet resistance, however, remained more or less consistent for thicknesses above 750nm which indicates that higher thicknesses are not needed to achieve a decent 10-12 Ω square sheet resistance. The TCO leak test was then performed from which it was determined that the TCO leak test also appeared to increase with the increase in the thickness of the TCO. However, in this test, the untreated samples had higher leak times than pre-treated samples which could be due to the higher presence of cracks or pinholes on the pre-treated samples.

Afterwards, structural characterizations such as confocal microscopy and SEM took place during which the roughness of the TCO as well as its uniformity and quality was determined. From the confocal microscopy analysis, the pre-treated samples appeared to be much rougher than the untreated samples.On the other hand, from the SEM images, the presence of particles called precipitants could be observed in pre-treated samples. Also, from the cross-sectional SEM images, the actual thickness from the SEM appears to match the optical TCO thickness determined from the APCVD diagnostics tool.Overall, from these characterizations, samples based of TCO thicknesses setting S1.5(790 nm) and setting S2.4(719 nm) overall appears to demonstrate better electrical and structural properties. As thickness appears to play a major role in the results so far, it was decided to make lab-scale samples based on S1.4(745 nm) and S2.4(720 nm) as they appeared to have similar thicknesses which will ensure better comparison between the untreated as well as the pre-treated samples. This experiment will be explained in detail in chapter 6.

5

Addressing the issue regarding the precipitants present in the Aluminium substrate at HyET Solar

This chapter focusses on strategies implemented in this thesis to address the issue regarding the presence of precipitants on HyET aluminium foils.Section 5.1 discusses the background and motivation behind the use of the pre-treatment process and the need to remove the precipitants from the aluminium foil. Section 5.2 discusses the experimental details, the observations as well as the results deduced from the acid treatments for the aluminium foil. Finally section 5.3 discusses the conclusions obtained through this set of experiments.

5.1. Background and Motivation

From the SEM analysis for the TCO layers in chapter 4, we could observe presence of precipitants scattered around the different areas of the aluminum substrate for the pre-treated samples. However, these precipitants do not appear for the untreated samples. The presence of these precipitants was observed for all the pre-treatment processes used which include factory baseline (FB) , FLAM01 and FLAM02. Overall, the pre-treated samples appeared to be rougher which was confirmed through the use of confocal microscopy in chapter 4.

However, despite these cons, the pre-treatment is necessary for texturing the foil to enhance light coupling into the cells which will enable generation of higher photocurrents thereby overall improving the efficiency of the solar modules. Previous experiments and simulations at HyET Solar demonstrate that the desired efficiencies greater than 12% on a tandem devices cannot be achieved without pre-treatment. Also, the presence of these precipitants is found on the active area after etching which could hinder the current potential of the HyET modules. These precipitants could also have a negative impact on the morphology, optical, and electrical properties of the PV modules thereby ensuring lower performance. Therefore, in order to reach the desired efficiencies at HyET, it is essential to eliminate or greatly reduce their number in order to ensure a homogeneous surface for the depositions of the TCO and silicon layers. Their homogeneous deposition could overall lead to better performance gains.

Overall, the precipitants could be removed by either aluminium stretching or acid treatment. Among these processes, the acid treatment has been found to be the most reliable process towards removal of these precipitants which could also be replicated on production scale. This acid treatment is usually performed post the pre-treatment process with NaOH solution.EDX analysis has been carried out to determine the composition of the precipitants which will help determine the best approach to eliminate them.

5.2. Experimental Details, Observations and Results

EDX analysis was carried out to determine the composition of the precipitants. Before getting the EDX analysis, a set of preliminary analysis was carried out as follows:

- Variation of baseline acid (H_3PO_4) from 1-75 w/w%

- Variation of different acids

In the first preliminary experiment, the baseline H_3PO_4 acid was varied from 1 to 75 w/w% of acid. The samples used for all the experiments is the Al foil with a thickness of 140 microns. The samples were first pre-treated with FLAM02 texture as it exposes larger number of precipitants. Afterwards,the samples were dipped in the acid bath for 12 seconds which serves as the current baseline.The temperature of the acid bath was set at 60°C which is the baseline temperature of the acid bath at HyET Solar. After the acid treatment, the samples were then taken to Delft where SEM was done to observe if the precipitants were removed from the aluminum surface.

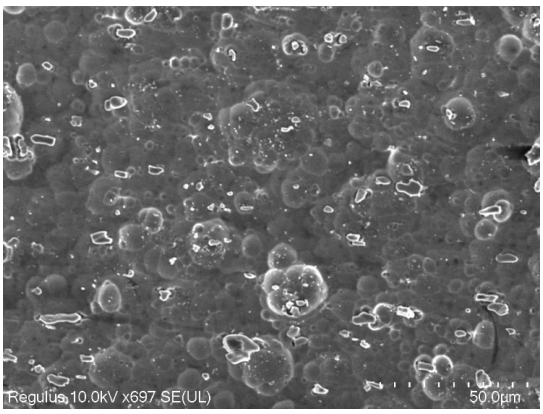

(a) 1 w/w% H_3PO_4

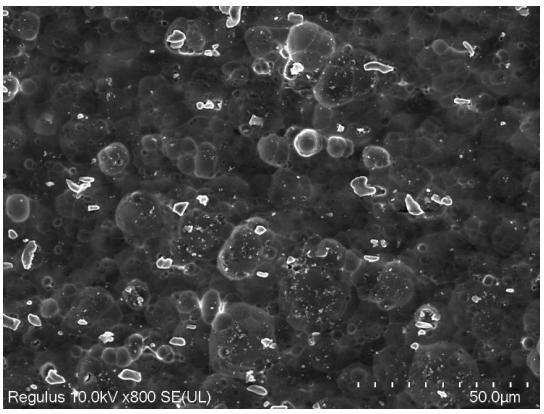

(b) 5 w/w% H_3PO_4

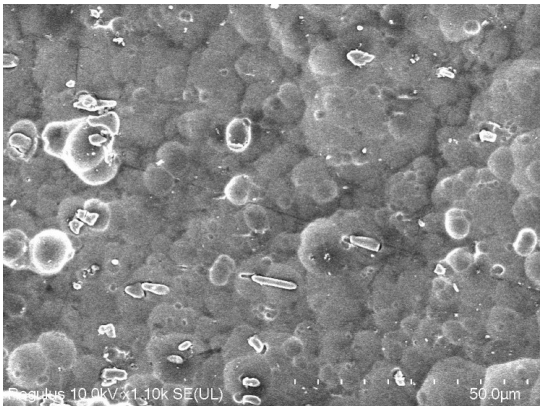

(c) 10 w/w% H_3PO_4

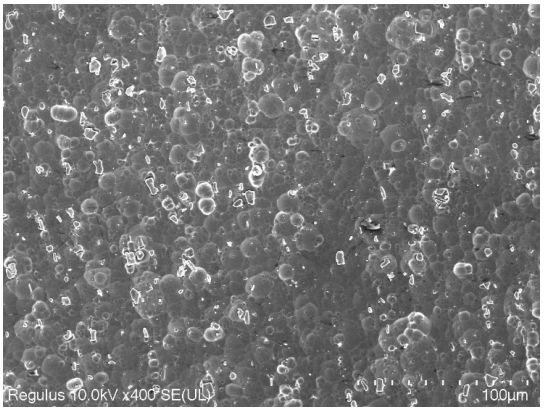

(d) 15 w/w% H_3PO_4

Figure 5.1: Variation of Baseline H_3PO_4 acid treatment between 1-15 w/w%

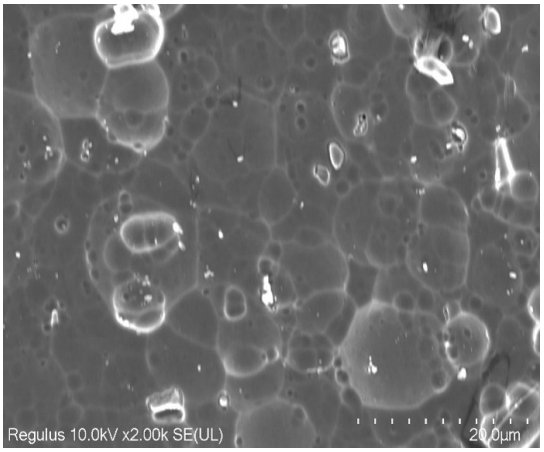

(a) 25 w/w% H_3PO_4

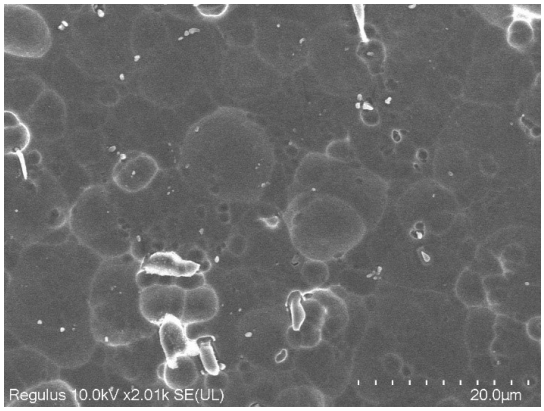

(b) 50 w/w% H_3PO_4

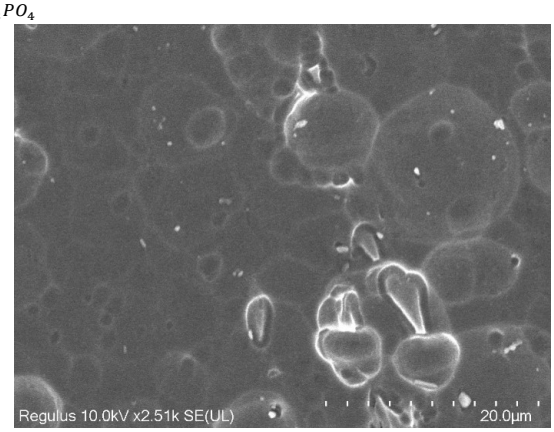

(c) 75 w/w% H_3PO_4

Figure 5.2: Variation of Baseline H_3PO_4 acid treatment between 25-75 w/w%

The SEM images were then taken for the above-mentioned samples which are shown above in figures 5.1 and 5.2 .It can be observed that the precipitants remain and are not removed for all the samples dipped in various baths. The precipitants do appear to be removed slightly for higher concentrations of 50 and 75 w/w% of H_3PO_4 acid although this will not be optimal from a production perspective as higher concentrations could cause overheating of the baths. Therefore, these results indicate that perhaps stronger acids could be tried to remove the precipitants.

Therefore, for the next experiment, it was decided to vary the acids and try different acids such as HNO_3, HCl and H_2SO_4 which could help in eliminating the precipitants. The molarity of all the acids were kept constant at 0.1 M.The rest of the parameters and conditions were kept constant as the first experiment. From the SEM analysis carried out in figure 5.3, the presence of precipitants was observed for each of the samples dipped in various acids. Therefore, the precipitants were not removed by using different acids as well. Therefore, the EDX analysis was then done for the samples which will help determine the composition of the precipitants. The EDX analysis was carried out in Delft with the help of the SEM Hitachi 8230 and the analysis of the data was done using the Fityk software to fit the peaks to determine the composition of the elements. The EDX analysis was done on areas without the precipitants, areas between the precipitants as well as on the precipitants lying across several different textured samples. The EDX analysis as well as the elemental composition of the precipitants are given below in figures 5.4 and 5.5.

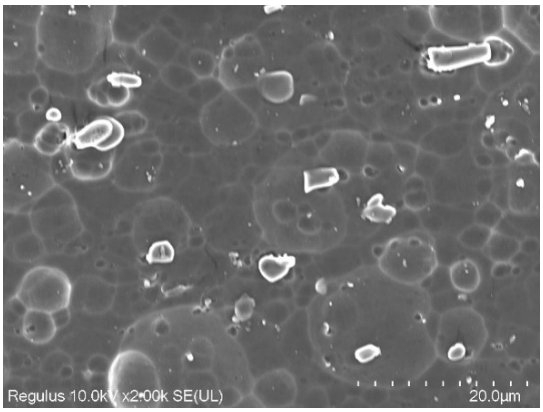

(a) 0.1 M HNO_3

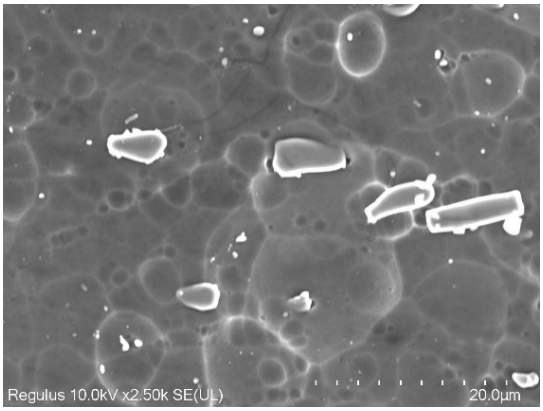

(b) 0.1 M H_2SO_4

1

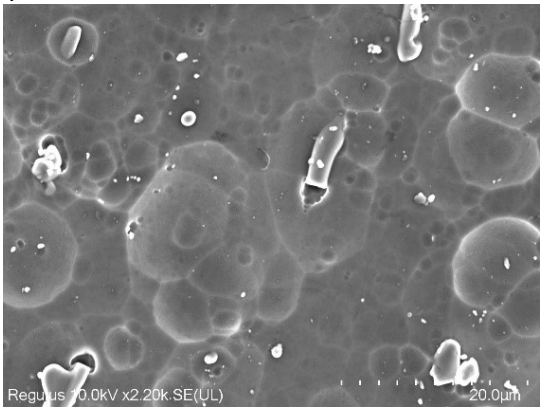

(c) 0.1 M H_3PO_4

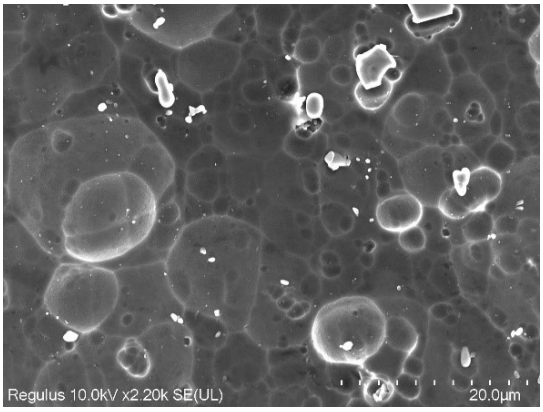

(d) 0.1 M HCl

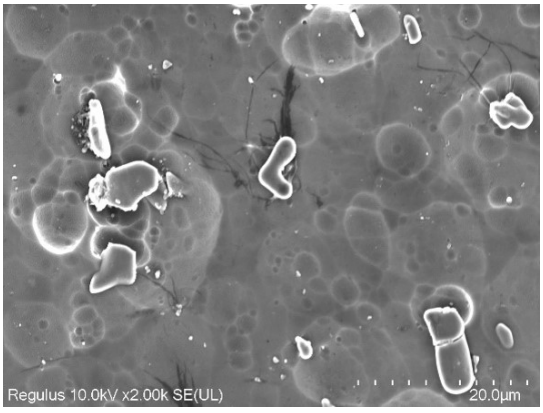

(e) No acid treatment

Figure 5.3: Variation of acids

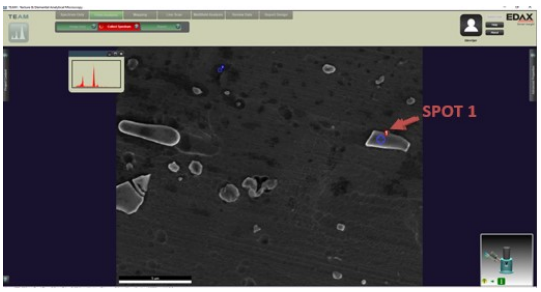

(a) EDX analysis on spot 1

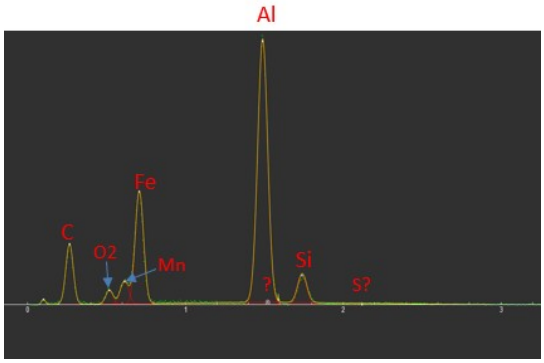

(b) EDX analysis fitting for spot 1 using fityk software

Figure 5.4: EDX analysis for spot 1

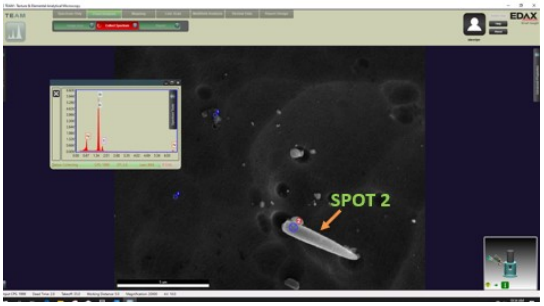

(a) EDX analysis on spot 2

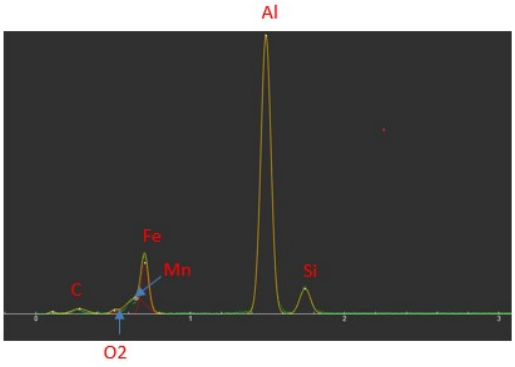

(b) EDX analysis fitting for spot 2 using fityk software

Figure 5.5: EDX analysis for spot 2

The average size and composition of the different measurements was calculated, and the results are highlighted below in table as follows:

S No.	EDX analysis Type	Average size(μm	Average (%) of precipitants
1	without the precipitants	-	Al(92.99%), Si(4.33%), C(1.82%)
2	between the precipitants	Less than 1	Fe(12.22%), Si(4.1%), Mn(3.13%)
3	on the precipitants	1-5	Fe(9.75%), Mn(5.98%), Si(4.53%)

Table 5.1: EDX analysis on areas without, between and on the precipitants

From the table above, the composition of the precipitants appears to be mainly Fe (concentration 9.75 +/- 7.27 %) followed by Mn (concentration 5.98 +/- 2 %) and Si (concentration 4.53 +/- 2.53%) and the size of the precipitants on average varies from less than 1 µm to a maximum of around 5-6 µm. In HyET Solar, the aluminum foil used for the production process is not 100% pure and usually a small quantity of elements such as iron, manganese and silicon are doped in it to boost its mechanical properties. This doping process is essential for the Al foil to be stable during the TCO as well as the silicon depositions. Therefore, these elements are what constitute the precipitants and it appears that the pre-treatment process exposes these precipitants when the aluminium etching takes place.

Therefore, a literature study was done on the different etchants which could help in removing these precipitants. Emphasis was laid on removing iron as it had the highest composition among all the precipitants while also ensuring that the aluminium foil is resistant to the etchant solution. Therefore, nital [72] and PES etchants [73] were tried in the next experiment due to their selectivity towards removing metals, particularly iron while ensuring that aluminium is resistant against them. The texturing used

(a) 12 sec dip

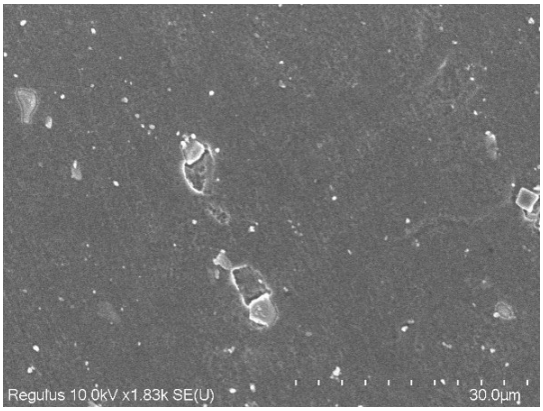

(b) 1 min dip

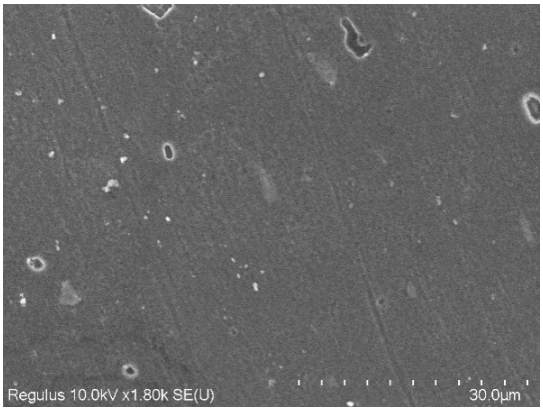

(c) 3 min dip

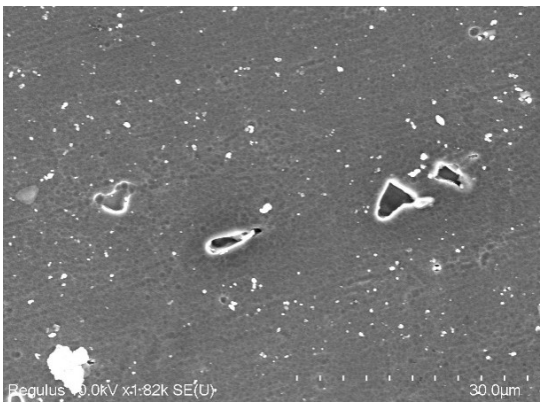

(d) 5 min dip

Figure 5.6: PES etchant acid treatment

was the FB texturing as it was the baseline process used at HyET and better analysis of the precipitants could be done using this texture compared to the FLAM01 or FLAM02 texture. The concentration was kept as per [73] for the PES etchant while the concentration of nital was kept at 2 w/w% since it was not recommended to use higher concentrations of nital due to its highly reactive nature [74]. The times of dipping in the etchants were varied for each of the acids from 12 seconds to 5 minutes.SEM images were taken for both the PES as well as the nital etchants to observe whether they are able to remove the precipitants or not.

From the SEM images in figures 5.6 and 5.7, we can observe that while the precipitants do not appear to be removed with nital etchant, it appears to be removed with the help of PES etchant when the samples were dipped at intervals of 3 and 5 min.Therefore, a further literature study was conducted to study the different methods which can help in removal of particles ranging in microns. From [75], it was found out that ultrasonication is a good method for removing particles especially in the order of microns if the right frequency is selected. The frequency required for removing particles of different sizes is highlighted in figure 5.8.

From figure 5.8, it was observed that frequencies from 100 to 400 kHz was ideal for removing particles ranging in size of 1 to 10 microns [75]. Therefore, an experiment was performed in which the acid was kept at baseline conditions and the samples were dipped in baseline H_3PO_4 acid baths with and without ultrasonication to observe if the precipitants were indeed being removed by ultrasonication. The ultrasonication frequency was kept at 130 kHz as that was the highest ultrasonicator frequency available at HyET Solar. Also, the time for dipping the sample in the acid bath was varied for 12 seconds and 3 min. The rest of the parameters were kept constant and the SEM images can be found in figure 5.9.

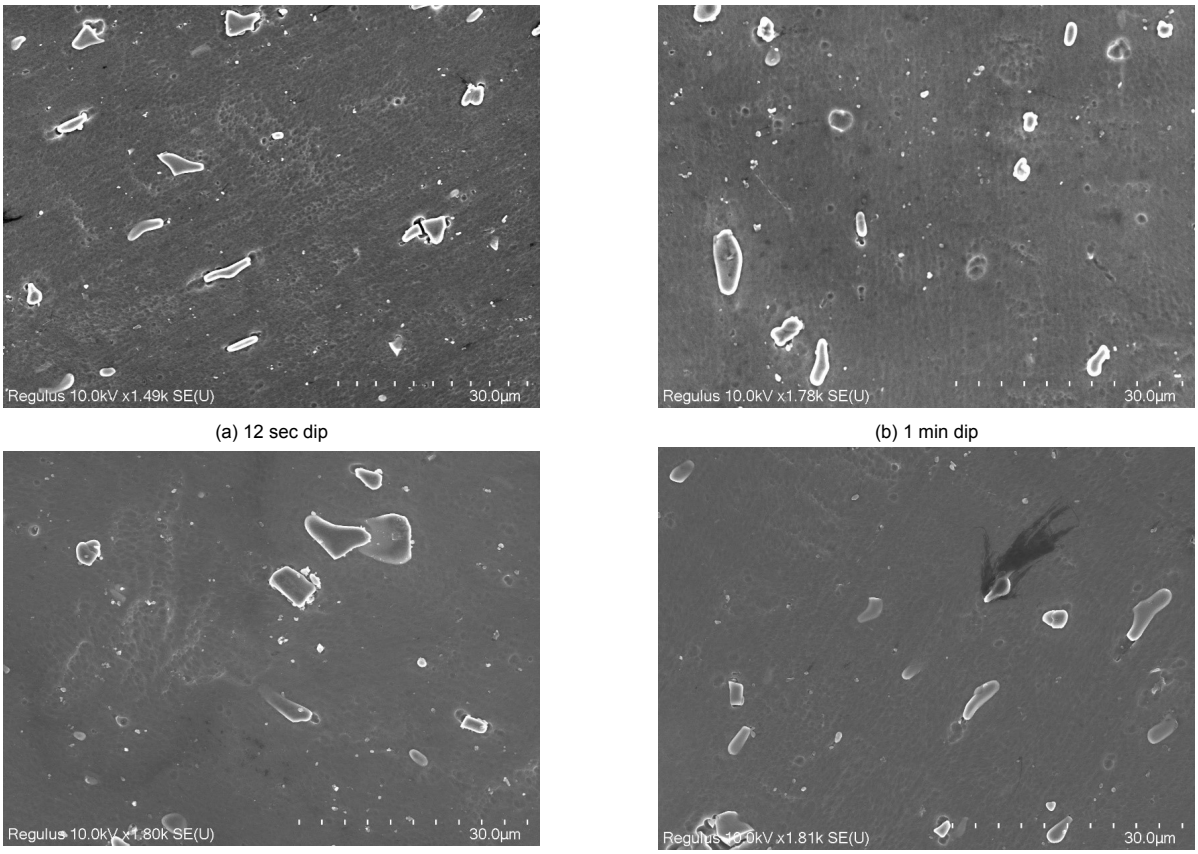

(a) 12 sec dip

(b) 1 min dip

(c) 3 min dip

(d) 5 min dip

Figure 5.7: Nital etchant acid treatment

Selecting the frequency

Frequency	Contamination	Applications	Damage	Characteristics
28kHz	Oil, visible contamination, large contamination	Degreasing metal parts, degreasing resin parts	Big	Used to remove persistent contamination such as grease, due to the strong cleaning energy. Enhances the effectiveness of the cleaning liquid.
40kHz	Contamination over 10 µm, dust	Initial cleaning of LCD glass, cleaning precision metal parts		Often used to clean precision parts, since there is less damage to the workpiece than at 28 kHz.
75kHz ≀ 100kHz	Over 5 µm - 10 µm	Cleaning HDD, CSP boards, precision metal parts, optical disks, HD heads		Often used if there is damage to the workpiece at 40 kHz. This frequency has recently gained attention due to the relatively strong cleaning energy and less damage to the workpiece.
120kHz ≀ 160kHz	1 µm - 10 µm	Compound wafers, HDD		Used to perform initial cleaning of wafers. Possible to remove fine contamination with minimal damage to the workpiece.
400kHz	0.2 µm~5 µm	Silicon wafers, glass wafers, glass substrate		May be suitable for various types of precision cleaning, due to the ability to remove a wide range of particle sizes.
1MHz	0.2 µm - 1 µm	Final cleaning of glass substrate, silicon wafers (with circuit), glass masks		Used to remove small particles that are not visible to the naked eye. Less damage to the workpiece. Widely preferred as the frequency to use for wafer cleaning.
3MHz	Below 0.2 µm	Silicon wafers (with circuit), glass masks	Small	Used to remove finer particles than at 1 MHz. Gaining attention as a new type of cleaning, due to particle acceleration that is stronger than at 1 MHz.

Low ↓ High

* 1 MHz particle acceleration = 10^5G (100,000 times the gravitational acceleration of Earth)

Figure 5.8: Importance of frequency in ultrasonication [75]

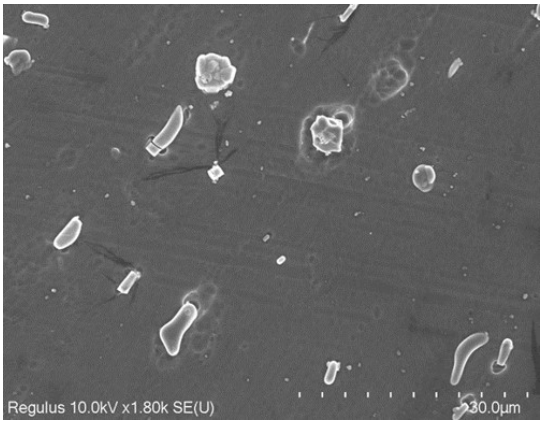

(a) 12 sec dip, no ultrasonication

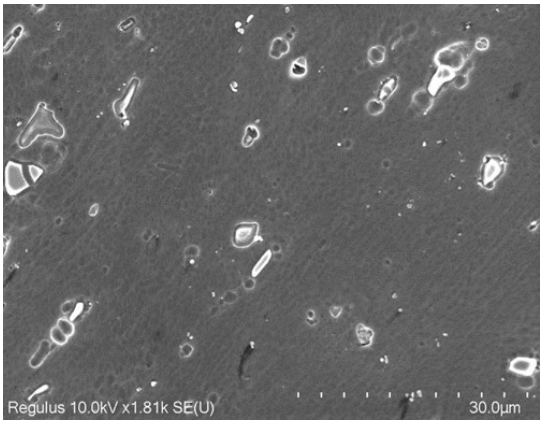

(b) 3 min dip, no ultrasonication

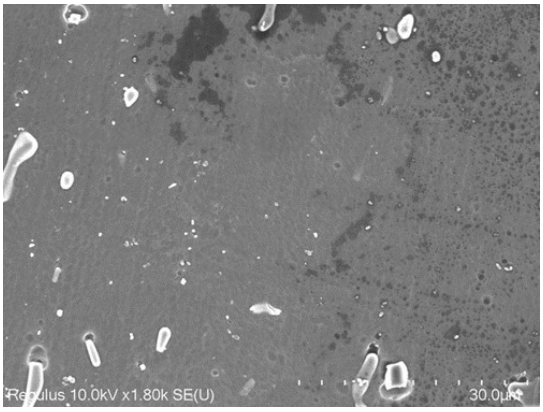

(c) 12 sec dip, ultrasonication

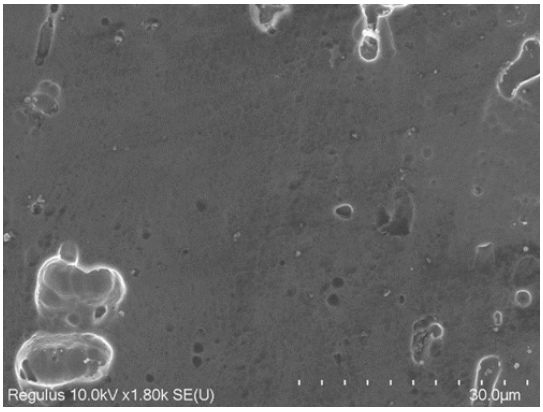

(d) 3 min dip, ultrasonication

Figure 5.9: Comparison between ultrasonicated samples vs samples with no ultrasonication

From the SEM images shown in figure 5.9, the presence of precipitants can be observed after 12 sec acid dip for both the ultrasonicated as well as the non-ultrasonicated bath. However, at 3 min acid dip, it can be observed that the precipitants do appear to be removed for the ultrasonicated bath, although the precipitants do appear to leave behind depth like structures. However, the results from ultrasonication are highly encouraging as it ensures the removal of the precipitants.

Therefore, based on the results from the ultrasonication run, it was decided to perform a time series variation for the acid treatment. Like the last experiment, 5 w/w% H_3PO_4 was ultrasonicated at 130 khz frequency at 60°C. The time of dipping the sample in the acid was varied for intervals of 12 sec, 1 min, 3 min and 5 min to observe the optimal time during which the precipitants are getting removed from the aluminium sample. FB texturing was done before the acid treatment and afterwards, SEM images were taken for the samples and is depicted below in figure 5.10.

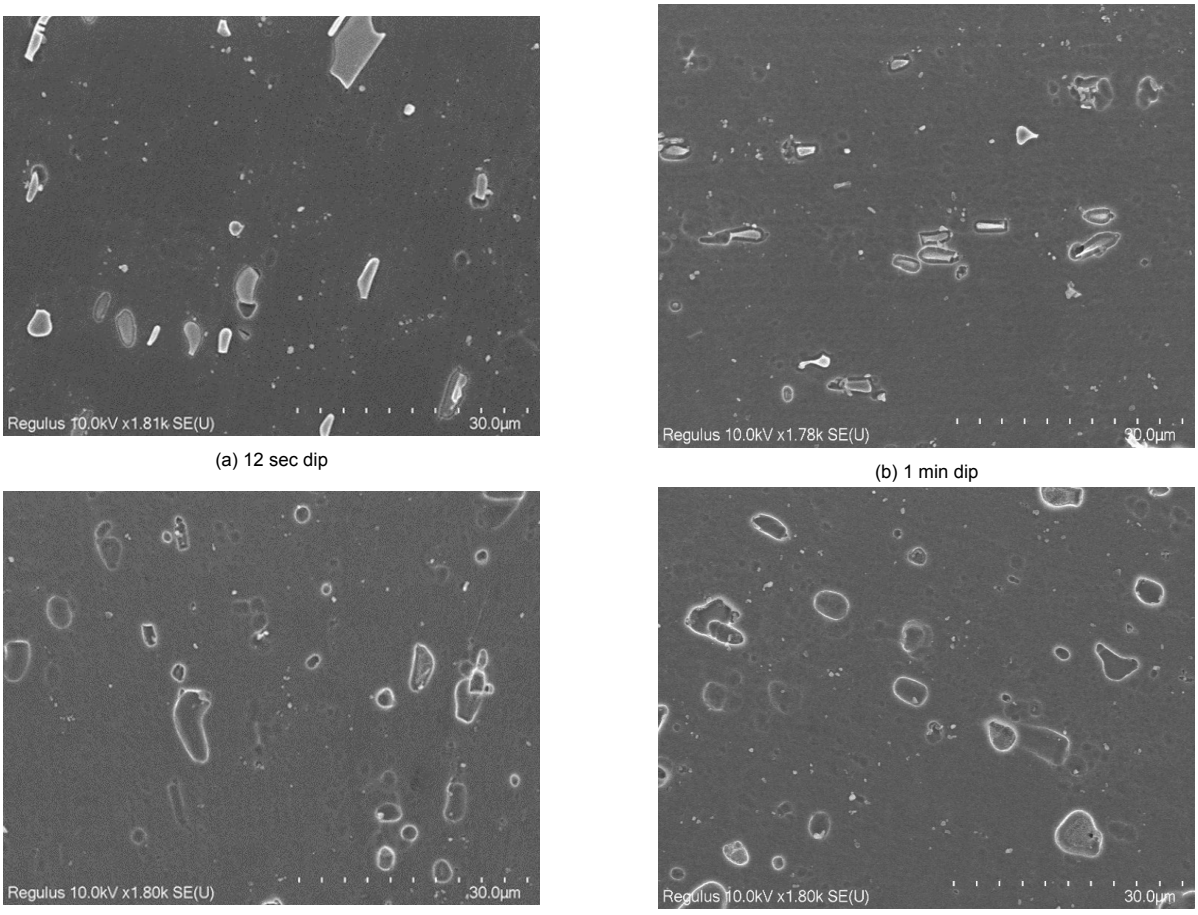

(a) 12 sec dip

(b) 1 min dip

(c) 3 min dip

(d) 5 min dip

Figure 5.10: Time Variation series for 5 w/w% H_3PO_4

From the SEM images shown in figure 5.10, the presence of the precipitants can be observed at 12 seconds dip. However, during the dip time of 1 min, there appears to be partial removal of the precipitants, but the surface appears uniform and free from holes observed in the previous experiment. However, at intervals of 3 and 5 min, the precipitants seem to be completely removed and holes seem to form in the place of the precipitants. The holes appear to be larger and sharper at the time interval of 5 min which may indicate etching of aluminium as well along with the precipitants removal.

In the next experiment, it was decided to vary the concentrations of the H_3PO_4 acid to observe if the higher concentration would help in removing the precipitants more quickly. Therefore, the concentrations were varied at 5 w/w% H_3PO_4 and 10 w/w% H_3PO_4. The time for dipping the samples was kept for 12 sec and 3 min. The rest of the parameters were kept constant, and the SEM images for this

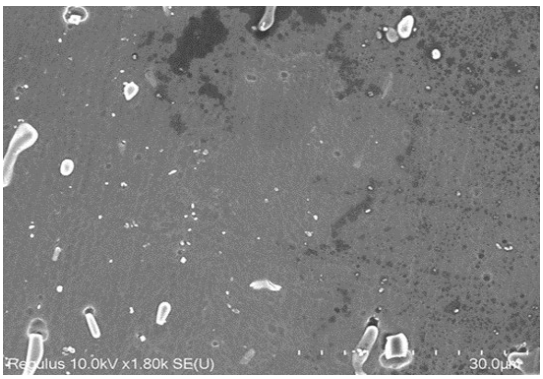

(a) 5 w/w%H_3PO_4, 12 sec dip

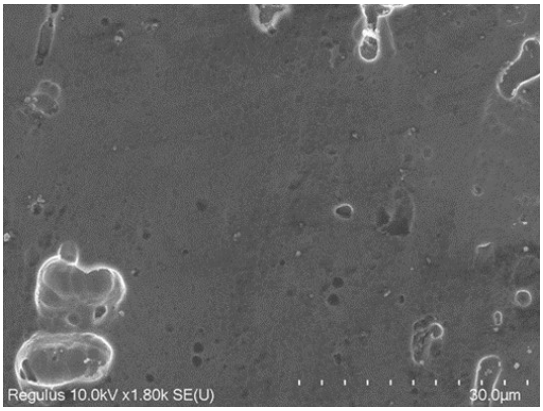

(b) 5 w/w%H_3PO_4, 3 min dip

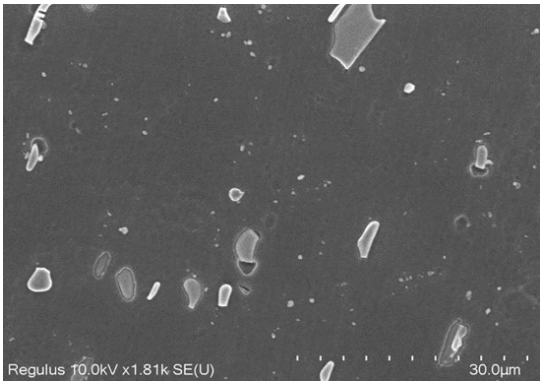

(c) 10 w/w%H_3PO_4, 12 sec dip

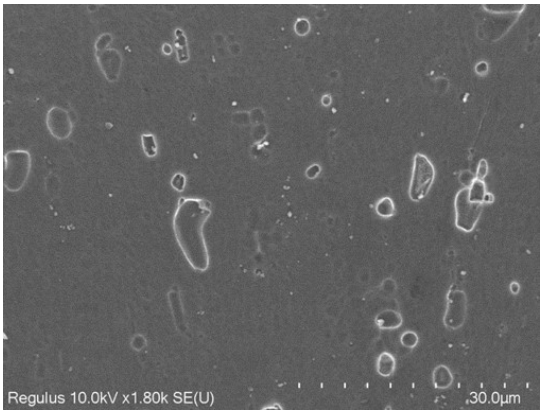

(d) 10 w/w%H_3PO_4, 3 min dip

Figure 5.11: Comparison between 5 and 10 w/w%H_3PO_4

experiment can be observed in figure 5.11. From the SEM images shown in figure 5.11, it can be observed that both 5 and 10 w/w% H_3PO_4 solutions appear to remove the precipitants at time interval of 3 min. However, worryingly, the presence of holes appears to be larger for samples dipped in 10% H_3PO_4 solution. Therefore, despite the removal of the precipitants, the holes are a major worry as they may create cracks on TCO and silicon layers,which could contribute to shunts.

From [76], it was observed that HNO_3 acid lowers the etching rate of aluminium.Therefore it could be used to prevent the formation of holes. Therefore, in the next experiment, acid baths of 5 w/w% H_3PO_4 were made which were then mixed in acid baths of 5 and 10 w/w% HNO_3. The time for dipping in the acid bath was kept for 12 sec and 3 min. The rest of the conditions were kept constant to the previous experiments. The SEM images of the samples from this experiment can be observed below in figure 5.12.

From the SEM images illustrated in figure 5.12, the acid mixture of 5 w/w% of HNO_3 and 5 w/w% of H_3PO_4 appears to remove the precipitants without the formation of holes. This result appears to be highly encouraging as it appears to remove the precipitants while ensuring a smooth surface for the deposition processes. Hence, it was decided to perform a confirmatory test using all the three textures at HyET Solar to observe if reproducible results can be achieved. Therefore, in the next experiment, the samples were taken from two random areas of the aluminium roll, which is named as batch A and batch B. All the three textures were performed for both the batch A and batch B samples and the time interval for the samples in the acid bath was kept as 3 min as this time interval has given the most promising results so far. The SEM images for the samples can be observed in figures figures 5.13, 5.14 and 5.15.

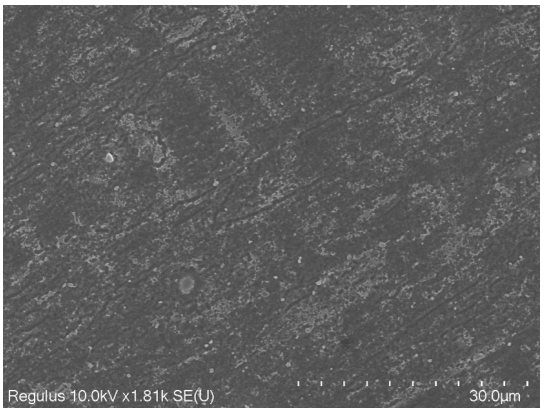

(a) 5 w/w% H_3PO_4 and 5 w/w% HNO_3, 12 sec dip

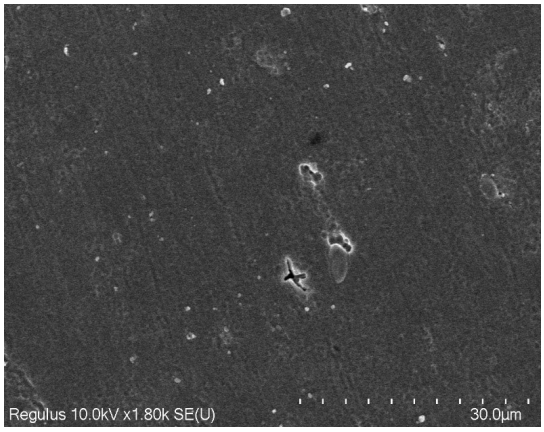

(b) 5 w/w% H_3PO_4 and 5 w/w% HNO_3, 3 min dip

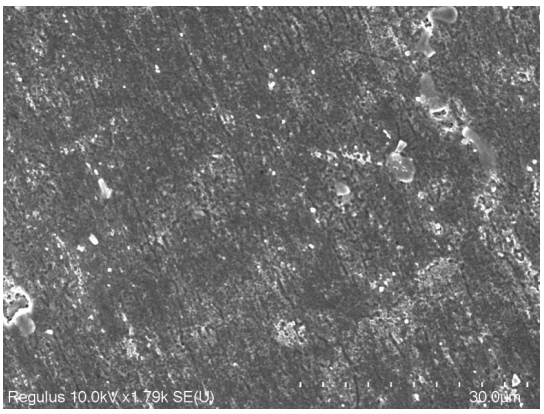

(c) 5 w/w% H_3PO_4 and 10 w/w% HNO_3, 12 sec dip

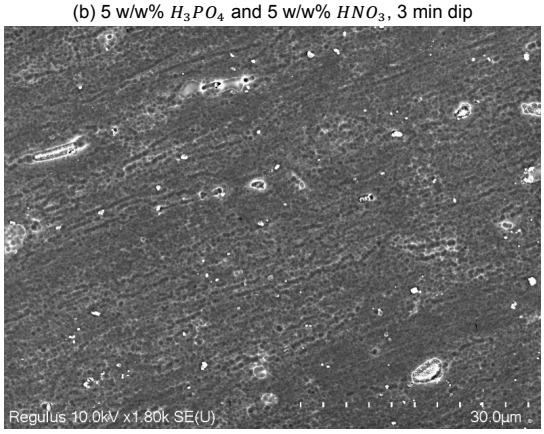

(d) 5 w/w% H_3PO_4 and 10 w/w% HNO_3, 3 min dip

Figure 5.12: Variations of mixture of H_3PO_4 and HNO_3

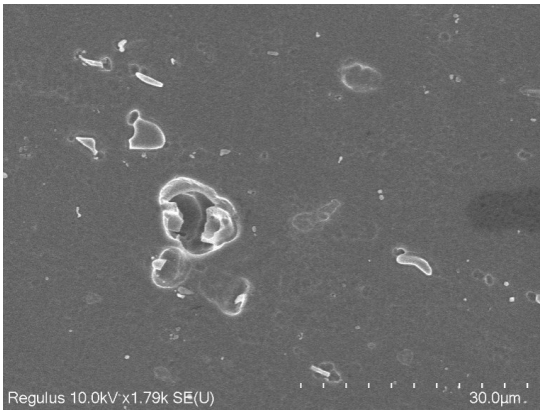

(a) FB Texture, Batch A

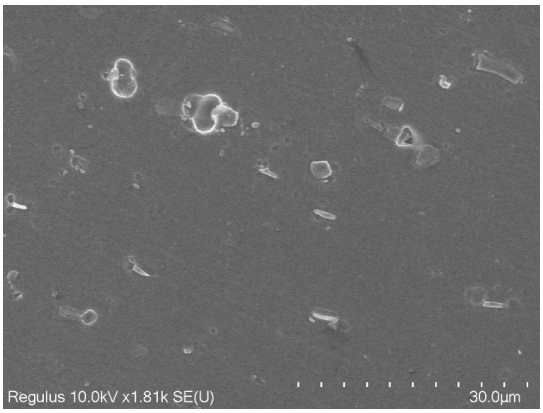

(b) FB Texture, Batch B

Figure 5.13: Factory Baseline Texture(FB) for confirmatory test of mixture of H_3PO_4 and HNO_3

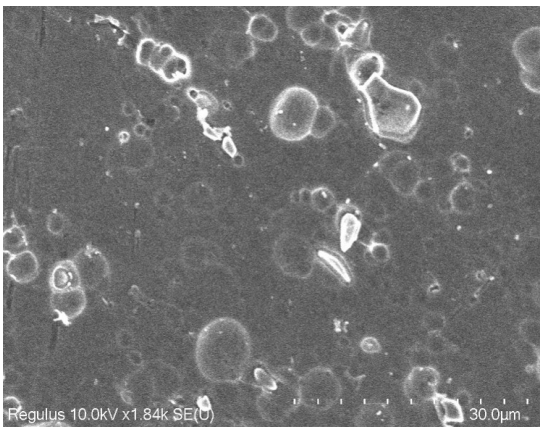

(a) FLAM01 Texture, Batch A

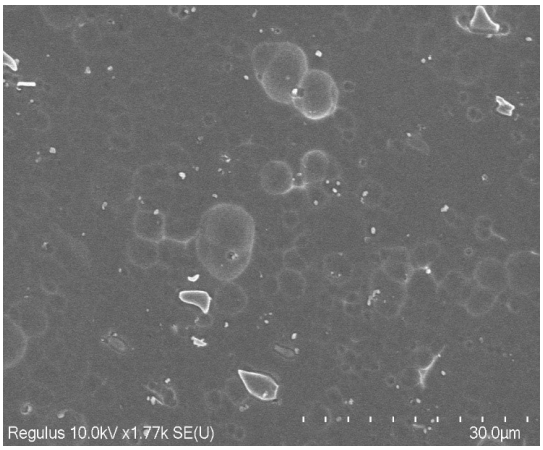

(b) FLAM01 Texture, Batch B

Figure 5.14: FLAM01 Texture for confirmatory test of mixture of H_3PO_4 and HNO_3

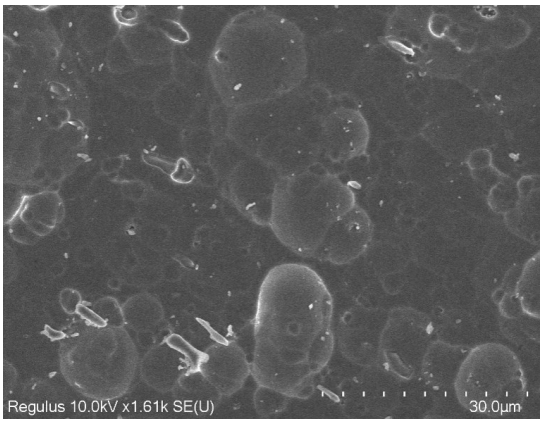

(a) FLAM02 Texture, Batch A

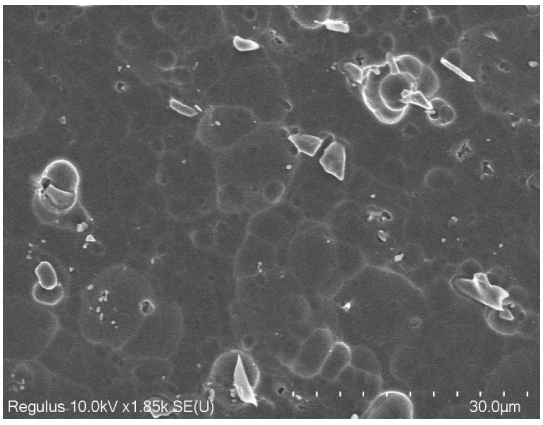

(b) FLAM02 Texture, Batch B

Figure 5.15: FLAM02 Texture for confirmatory test of mixture of H_3PO_4 and HNO_3

From the SEM images depicted in figures 5.13, 5.14 and 5.15, the precipitants unfortunately still appear to be present in samples with all the three different textures across both batch A and batch B of the samples. This indicates that the H_3PO_4 and HNO_3 acid mixture failed to satisfy the confirmation test as

reproducible results could not be achieved.

In the next experiment, it was decided to do an experiment in which the different acids were varied.4 different acid solutions- H_3PO_4, HNO_3, HCl and H_2SO_4 were taken and the concentration for each of the acids was kept at 5 w/w% of the acid which were ultrasonicated at a frequency of 130 kHz.The samples were textured with the baseline FB texture before undergoing the acid -treatment. The rest of the conditions were kept constant to the previous experiments. The SEM images for the samples of this experiment are given below in figure 5.16. The SEM images are only shown for the H_3PO_4, HNO_3 and H_2SO_4 acids as the sample dipped in HCl acid bath was dissolved completely by the acid.

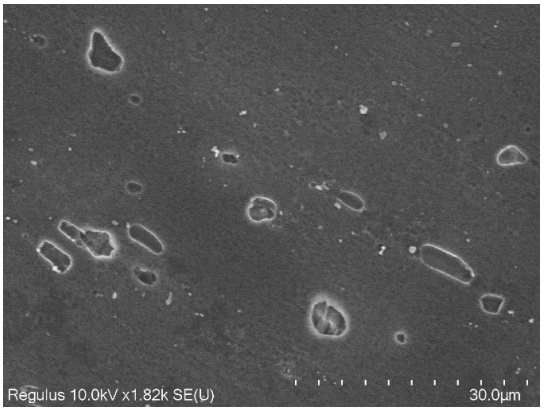

(a) 5 w/w% H_3PO_4, 3 min dip

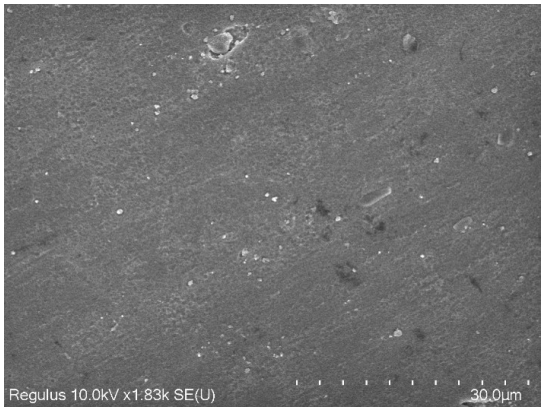

(b) 5 w/w% HNO_3, 3 min dip

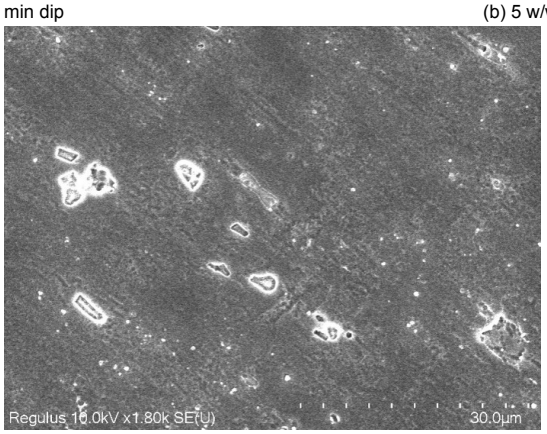

(c) 5 w/w% H_2SO_4, 3 min dip

Figure 5.16: Acid Treatment using various acids with ultrasonication

From the SEM images shown in figure 5.16, it can be observed that 5 w/w% of H_3PO_4 and HNO_3 helps remove the precipitants. The sample dipped in 5 w/w% of H_3PO_4 does appear to show similar hole features as observed in the previous experiments, but 5 w/w% of HNO_3 appears to remove the precipitants without the formation of holes which is seen for the H_3PO_4 acid. This result is highly encouraging as it shows that it can remove the precipitants while ensuring a homogeneous surface for future TCO and silicon depositions. Therefore, a confirmatory test similar to mixture of H_3PO_4 and HNO_3 acid bath needs to be carried out for the 5 w/w% HNO_3 acid bath.

5.3. Conclusions

Overall, different sets of acid treatments were carried out in order to remove the precipitants.The EDX analysis was done on the precipitants through which it was found that iron, silicon, and manganese were the main elements present in it.Also,the samples dipped in ultrasonicated acid baths appeared to show less precipitants than the samples dipped in acid baths without ultrasonication. It was also observed that the removal of precipitants was mainly observed for the acid treatments with H_3PO_4, HNO_3 and PES etchant. From the time variation experiments, it was observed that the H_3PO_4 acid and the PES

etchant appeared to remove the precipitants from the aluminium foil but left behind holes. Also, the mixture of 5 w/w % of H_3PO_4 and HNO_3 acid treatment showed promising initial results as it appeared to remove precipitants while ensuring a homogeneous surface, but it failed the confirmatory test which was done for all the three textures. Overall, from these set of experiments, it can be concluded that ultrasonication process in acid baths currently appears to be the best method in order to reduce the number of precipitants which are currently present in the aluminium foil at HyET. However, the best treatment for ensuring the overall improvement of PV performance is yet to be determined.

6

Lab Scale Production of HyET Modules

Section 6.1 introduces the background and motivation behind performing this experiment. It also emphasizes on the production of the single cell lab scale modules at HyET Solar.Section 6.2 explains the production process of the single cell modules based on the results obtained from chapter 4.Sections 6.3 discusses the results of the measurements of dark JV, light JV and EQE which had been done on these lab modules.Section 6.4 depicts the overall conclusions gained from performing this experiment.

6.1. Background and Motivation

HyET Solar aims to obtain 7-8% stabilized efficiency for single junction and 12% stabilized efficiency for tandem modules. Therefore, to achieve these aims, several layers need to be re-optimized to meet these efficiency targets. In chapter 4, emphasis had been laid to optimize and characterize the TCO layer at HyET based on which TCO layers of setting 1.4(745 nm untreated Al) and setting 2.4(720 nm pre-treated) were selected to make lab-scale solar devices. Making lab scale solar cells using these TCO settings and comparing them versus the existing solar cells would give HyET a better understanding regarding the quality of the TCO. Hence, to confirm the findings from the TCO experiment, it was decided to make tandem as well as single junction solar cells on the optimized TCO samples for both the untreated as well as the pre-treated roll. The type of samples made were single cell modules (SCM) as they offer a realistic demonstration of the actual production modules by HyET. Also, active areas can be varied in this configuration which will give a better idea regarding the impact of the cell area on the overall performance. Figures 6.1 and 6.2 below highlight the top side as well as the cross-sectional view for the lab modules processed in this thesis.

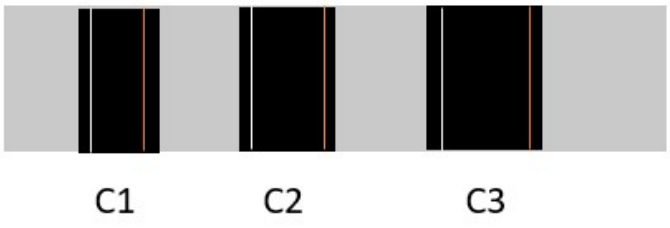

Figure 6.1: Single cell modules(SCM) top view

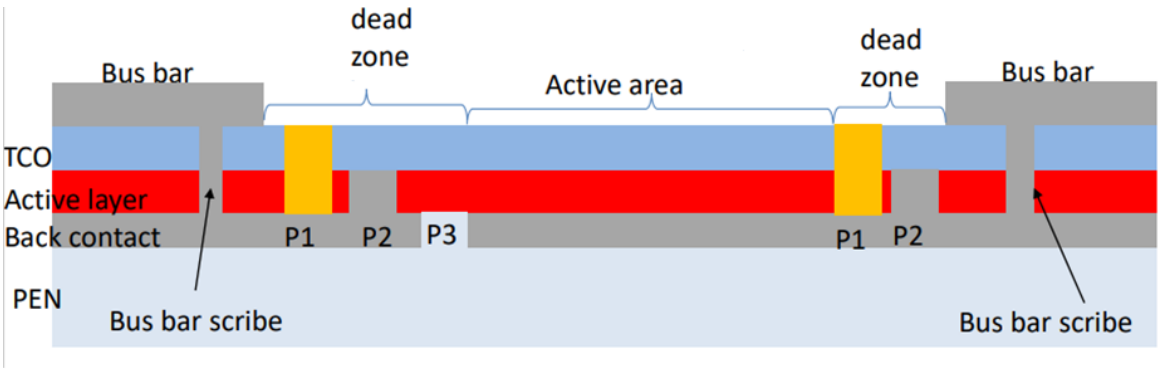

Figure 6.2: Single cell modules cross-sectional view

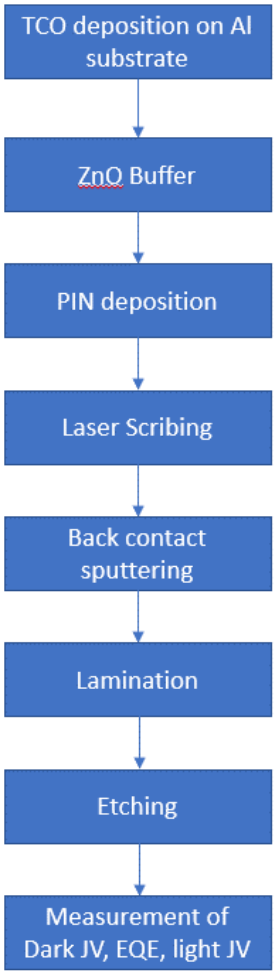

Figure 6.3: Procedure for making cells on Foil(COF) lab scale devices

6.2. Experimental Details

The experimental procedure for making lab scale solar cells from TCO on aluminium substrate is highlighted in the flowchart in figure 6.3. The selected TCO settings (S1.4 and S2.4) samples were sent to TU Delft where the ZnO buffer layer was deposited by RF sputtering while the silicon PIN layers were deposited afterwards using the PECVD (Plasma enhanced chemical vapor deposition) process.

For this thesis, the samples processed were tandem devices. Afterwards, the samples were taken to HyET Solar where the interconnections for the cells were done through laser scribing. Afterwards, the back contact sputtering of ZnO and Al took place using the RF sputtering and the DC sputtering method respectively. The samples were then laminated with the permanent plastic carrier foil (PEN). Afterwards, a two-step etching process took place with annealing in between to etch out the aluminium layer from the sample while preserving the TCO and silicon stack. After making the lab-based solar cells, dark JV measurements were carried out to measure the shunt resistance. Ideally, it is expected that a good working cell at HyET Solar has a shunt resistance of around 10 $K\Omega\ cm^2$. Afterwards, EQE was measured for the solar cells in order to measure the currents in both the top cell and bottom cell. Lastly, light JV was performed on the solar cells for measuring the overall performance of the cells. This measurement gives values of important performance parameters such as the open circuit voltage(V_{oc}), short circuit current density(J_{sc}), fill factor(FF) as well as the overall efficiency of the solar cells(η).

6.3. Observations and Results

After the deposition of the layers as well as the establishment of the interconnections, lab samples were then processed in the lab at HyET Solar. Afterwards, dark JV measurements were performed on the devices. Each sample consists of 3 cells which have active areas of 3, 4.5 and 6 cm^2. The 3 cells are named as A1,A2,A3 and B1,B2,B3 for the untreated as well as the pre-treated sample respectively. The dark J-V plot as well as the shunt resistances for each of the cells were measured and the results are shown below in figures 6.4 and 6.5 as follows:

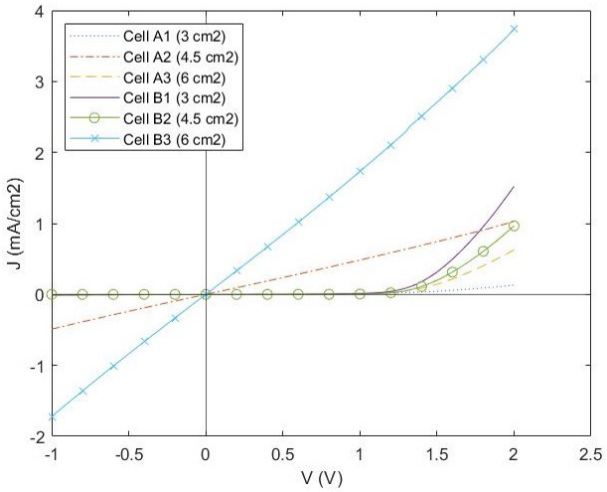

Figure 6.4: Dark JV measurement for SCM devices

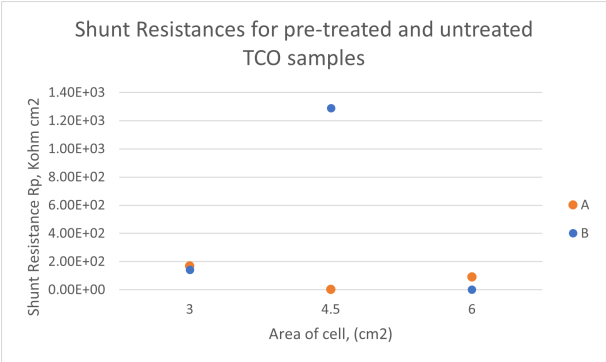

Figure 6.5: Shunt resistance measurement for SCM devices

From the dark JV analysis, it can be observed that the performance of the samples was very poor

and none of the cells across the untreated and the pre-treated sample demonstrated ideal J-V behaviour. However, the shunt resistances do appear encouraging for both the pre-treated as well as untreated samples which demonstrate shunt resistances of roughly 100 $K\Omega cm^2$.These results for the cells are well above the desired shunt resistance of 10 $K\Omega cm^2$.

Afterwards, the sample was measured in the EQE setup in order to determine the individual short circuit currents for both the top as well as the bottom cell for each sample.The EQE measurements for the top as well as the bottom cells for cells B1 and B2 of the pre-treated sample are shown below in figure 6.6. Unfortunately, the measurements appear to be extremely poor and the bottom cell appears to be too amorphous which could impact the J_{sc}. The table 6.1 shows the J_{sc} of the top as well as the bottom cell. Overall, both the top and bottom cell currents were extremely low and well short of the desired J_{sc} at HyET.

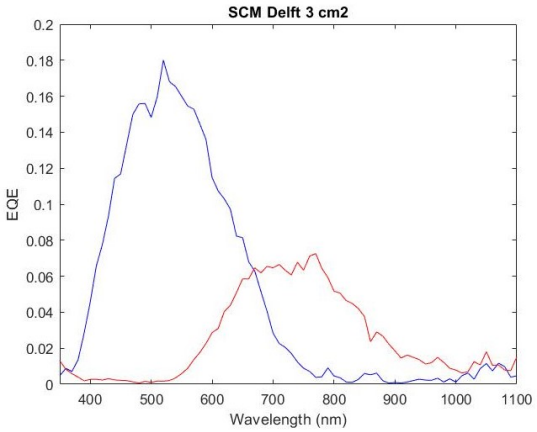

(a) EQE response for pre-treated sample, B1-3cm^2

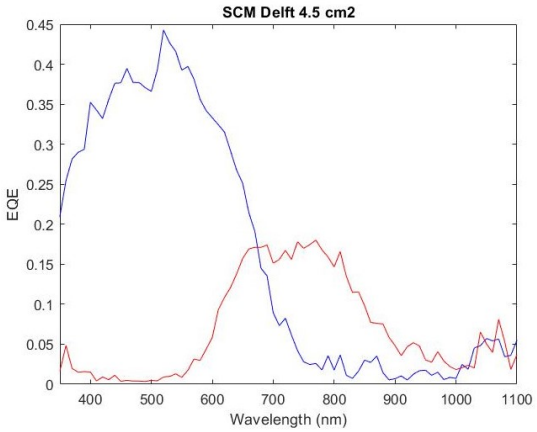

(b) EQE response for pre-treated sample, B2-4.5cm^2

Figure 6.6: EQE response for cells B1 and B2 of the pre-treated samples

Cell	Top Cell(mA/cm^2)	Bottom Cell(mA/cm^2)
B1	2.32	1.22
B2	6.79	3.3

Table 6.1: Top and Bottom cell currents for pre-treated sample from EQE

Light JV was also performed for both the samples. However, the cells across both the samples did not induce any performance. Therefore, the voltage of the samples was then measured using the voltmeter. However, the voltage performance for all the cells were poor and were well short of the desired voltages of around 1.3V for the tandem cells.

Cell	Type of Al foil	V(V)	Area(cm^2)
A1	untreated	0.11	3
A2	untreated	0	4.5
A3	untreated	0.12	6
B1	pre-treated	0.13	3
B2	pre-treated	0.38	4.5
B3	pre-treated	0	6

Table 6.2: Voltage measurement of SCM modules using the voltmeter

6.4. Conclusions

Overall, the best TCO samples with the best sheet resistance and leak time were chosen in order to make lab scale samples to observe if these TCO samples are able to deliver a better performance than

the samples with baseline TCO thickness. The samples were prepared in single cell modules(SCM) arrangement which provides an actual representation of the actual production modules. Once the samples were prepared, different measurements such as dark JV, light JV and EQE were performed. From the dark JV analysis, it was observed that the pre-treated samples were able to demonstrate good shunt resistances well above the minimum threshold of 10 $K\Omega cm_2$. The samples however failed to give desirable electrical characteristics in both light as well as dark JV measurements. Finally, the EQE measurements were performed which confirmed the low J_{sc} measurements present in both the top as well as the bottom cell. Overall, the lab samples failed to give reliable measurements for both untreated as well as pre-treated TCO samples.

7

Conclusions and Recommendations from the Thesis project

This thesis focused on the characterization of the TCO as well as improving the performance of the lab scale solar modules at HyET Solar. The FLAMINGO PV group aims to realise efficiencies of 12% for tandem solar modules and hence this thesis focuses on strategies particularly on the TCO quality and the aluminium surface morphology to fulfill the desired efficiencies required by the group.

Section 7.1 focuses on the conclusions gained from this thesis project while section 7.2 lays its emphasis on recommendations as well as future work which can be implemented to further improve the yield and performance of the lab-scale solar modules at HyET Solar.

7.1. Conclusions

Overall, from the TCO thickness variations, an efficient and reliable approach was set for characterization of the TCO at HyET Solar which will help the company in identifying the TCO characteristics in the near future.The focus of this thesis was mainly on the electrical and structural properties of the TCO which will make it easier for HyET to qualify the TCO. Optical properties unfortunately could not be explored as the aluminium substrate as well as the PEN substrate could not provide reliable transmission measurements. The TCO samples were first subject to the sheet resistance measurement during which it was found that desired sheet resistances of around 10-12 ohms sq were obtained mainly for the pre-treated samples. However, in the TCO leak test, the untreated samples appeared to show better leak times which could possibly be due to the lower concentration of pinholes or cracks in them compared to the pre-treated samples.Afterwards, structural characterizations such as confocal and SEM took place during which the roughness of the TCO as well as its uniformity and quality was determined. From the confocal microscopy analysis, it was observed that the pre-treated samples appear to have higher surface irregularities such as cracks or pinholes compared to the untreated samples.Through SEM, the presence of particles called precipitants could be observed in pre-treated samples which is tackled in chapter 5. Overall, from these characterizations, samples based on TCO thicknesses settings S1.5(790 nm) and setting S2.4(719 nm) overall gave better results compared to other TCO thicknesses.

Addressing the issue of the precipitants present in HyET aluminium foil was the next focus for this thesis. Before the EDX analysis, different concentrations of baseline acid H_3PO_4 (1-75 w/w%) as well as different acids (H_3PO_4, HCl, H_2SO_4 and HNO_3) were tried but they failed to eliminate the precipitants. Next, EDX analysis was done on the precipitants through which it was found that iron, silicon and manganese were the main elements present in the precipitants. Afterwards, it was found that ultrasonication was a suitable method for the removal of the precipitants. Overall, different acids were tried among which H_3PO_4, HNO_3 and PES etchant appeared to give the most promising results. It was also observed that a minimum time of three minutes was required for removing the precipitants using the above mentioned acids. Also, it was observed that the H_3PO_4 and PES etchant appeared to remove the precipitants from the aluminium foil but left behind holes especially for the time intervals

of 3 and 5 min. A mixture of 5 w/w% of H_3PO_4 and HNO_3 appeared to demonstrate really promising initial results as it appeared to remove precipitants while preventing the formation of holes, but it failed the confirmatory test which was done across the three different textures on two separate areas of the aluminium roll. Overall, ultrasonication seems to be the best method for the removal of the precipitants and based on [75], higher frequencies can be attempted in order to remove them.

In the final experiment,lab scale devices were made from the selected TCO samples to observe if these TCO samples are able to deliver a better performance than the samples with baseline TCO.The samples were prepared in single cell modules(SCM) arrangement which provides an actual representation of the production modules at HyET. Once the samples were prepared, different measurements such as dark JV, light JV and EQE were performed. From the dark JV analysis, it was observed that the pre-treated samples were able to demonstrate good shunt resistances well above the minimum threshold of 10KΩcm^2. The samples however failed to give desirable electrical characteristics in both light as well as dark JV measurements. Finally, the EQE measurements were performed which confirmed the low J_{sc} present in both the top as well as the bottom cell. Overall, the lab samples failed to give reliable measurements for both untreated as well as pre-treated TCO samples.

7.2. Recommendations and Future Work

Overall, the thesis highlighted the importance of optimizing the TCO as well as the aluminium surface morphology which could help in obtaining higher efficiencies of around 12% desired by HyET. In the TCO thickness variations experiment, the electrical as well as the structural properties of the TCO were studied. However, the optical properties especially the transmittance could not be explored in this thesis as the aluminium substrate as well as the PEN substrate could not provide reliable measurements. Hence, the deposition of TCO needs to be done on a transparent substrate such as glass which will thereby provide much more accurate measurements. Also, from [77], it was observed that the methanol as well as the HF flow rate can be tweaked to get desired electrical properties hence an experiment can also be conducted by varying these flow rates and observing their effect on the electrical properties.Currently, the TCO deposition occurs through a roll-to-roll process at HyET and hence a new batch APCVD reactor will soon arrive at HyET in which these experiments can easily be carried out.

In terms of addressing the issues regarding the precipitants, it was found that ultrasonication using 5% baseline H_3PO_4 acid proved to be the best bet for removal of precipitants for a minimum dip time of 3 min. However, while this managed to remove the precipitants, it also left behind holes which could influence the further depositions.As highly sharp features could develop cracks which will thereby induce shunts, AFM can be used in order to determine the depth/height of the precipitants and holes which will help determine their sharpness.Also, an experiment can be carried out to optimize the time of the sample dip between 1 and 3 min as this is the interval between which the precipitants are being removed while leaving behind holes. Also, currently all the ultrasonication experiments were tried at a frequency of 130 kHz as this was the highest frequency available at HyET. From [75], it could be observed that frequencies of above 400 kHz could be attempted to remove particles with an average size of 1-5 microns. Also, when the batch APCVD reactor gets operational at HyET, samples can be made with and without the acid treatment to observe the overall influence of the precipitants in the performance of the HyET modules.

In the last experiment, the selected TCO samples were processed into lab scale devices which overall yielded poor J_{sc} and V_{oc} measurements. Upon further exploration, through optical microscopy, it was found that the laser scribes were too deep which overall induced shunts which led to the poor performance of the modules. Therefore, the laser scribing overall needs to be optimized for tandem lab scale samples. Also, Raman spectroscopy can be implemented to check the overall crystallinity of the a-Si:H and nc-Si:H layers which were deposited by the batch PECVD reactor in Delft.

Overall, these recommendations can be implemented in order to improve the performance of the existing lab samples which will therefore be a good step forward towards achieving the desired efficiencies of 12% for tandem modules.

Bibliography

[1] International Energy Agency(IEA). *Solar Energy Perspectives: Executive Summary*. 2012. url: http://large.stanford.edu/courses/2016/ph240/sheu1/docs/iea-solar-2011.pdf.

[2] Royal Society of Chemistry(RSC). *Energy*. 2014. url: https://pubs.rsc.org/en/content/articlelanding/2014/ee/c3ee90052e/unauth.

[3] World Economic forum. *Renewables power ahead to become the world's cheapest source of energy in 2020*. 2020. url: https://www.weforum.org/agenda/2021/07/renewables-cheapest-energy-source.

[4] Lazard. *Levelized Cost Of Energy, Levelized Cost Of Storage, and Levelized Cost Of Hydrogen*. 2021. url: https://www.lazard.com/perspective/levelized-cost-of-energy-levelized-cost-of-storage-and-levelized-cost-of-hydrogen/.

[5] *Growth of photovoltaics*. 2018. url: https://en.wikipedia.org/wiki/Growth_of_photovoltaics.

[6] M. Askari M.and Mirzaei, V. Abadi, and M. Mirhabibi. "Types of Solar Cells and Application". In: *American Journal of Optics and Photonics* 6 (2015), pp. 289–306. doi: 10.11648/j.ajop.20150305.17.

[7] A. McEvoy, L Castaner, and T. Markvart. "Solar Cells: Materials, Manufacture and Operation". In: *Elsevier Ltd., Oxford* 3 (2012), p. 25.

[8] A.L. Fahrenbruch and R.H. Bube. "Fundamentals of Solar Cells". In: *Academic Press Inc., New York* (1983).

[9] B. Srinivas et al. "Review on Present and Advance Materials for Solar Cells". In: *International Journal of Engineering Research-Online* 3 (2015), pp. 178–182.

[10] P. Wurfel and U. Wurfel. "Physics of Solar Cells: From Basic Principles to Advanced Concepts". In: *John Wiley Sons, Hoboken* (2009).

[11] B. Srinivas et al. "Review on Present and Advance Materials for Solar Cells". In: *International Journal of Engineering Research-Online* 3 (2015), pp. 178–182.

[12] Office of energy efficiency and renewable energy. *Crystalline silicon photovoltaics research*. url: https://www.energy.gov/eere/solar/crystalline-silicon-photovoltaics-research#:~:text=Crystalline%5C%20silicon%5C%20PV%5C%20cells%5C%20have,22%5C%25%5C%20under%5C%20standard%5C%20test%5C%20conditions.

[13] T. Saga. "Advances in Crystalline Silicon Solar Cell Technology for Industrial Mass Production". In: *NPG Asia Materials* 2 (2010), pp. 96–102.

[14] K.L. Chopra, P.D. Paulson, and V. Dutt. "Thin-Film Solar Cells: An Overview." In: *Progress in Photovoltaics* 12 (2004), pp. 69–72.

[15] M. Imamzai et al. "A Review on Comparison between Traditional Silicon Solar Cells and Thin-Film CdTe Solar Cells". In: *Proceedings of National Graduate Conference* (2012), pp. 1–5.

[16] Material District. *Innovation:Thin film solar cells at MX2016*. 2016. url: https://materialdistrict.com/article/innovation-thin-film-solar-cells-at-mx2016/.

[17] W. Shockley and H. J. Queisser. "Detailed Balance Limit of Efficiency of p-n Junction Solar Cells". In: *Journal of Applied Physics* (1961), p. 510. doi: 10.1063/1.1736034.

[18] Antonio Luque and Gerardo López Araujo. "Physical Limitations to Photovoltaic Energy Conversion". In: *Hilger* (1990).

[19] Phys Org. *A new stable and cost-cutting type of perovskite solar cell*. 2015. url: https://phys.org/news/2014-07-stable-cost-cutting-perovskite-solar-cell.html.

[20] Royal Society of chemistry(RSC). *Spray-deposition steers perovskite solar cells towards commercialisation*. 2014. url: https://www.chemistryworld.com/news/spray-deposition-steers-perovskite-solar-cells-towards-commercialisation/7600.article.

[21] PV Magazine. *Unique properties of organic polymer solar cells expected to open niche market opportunities*. 2018. url: https://www.pv-magazine.com/2018/02/23/unique-properties-of-organic-polymer-solar-cells-expected-to-open-niche-market-opportunities/.

[22] Fraunhofer ISE. *Photovoltaics Report(PDF)*. 2014. url: https://www.ise.fraunhofer.de/content/dam/ise/en/documents/annual_reports/Fraunhofer_ISE_Annual_Report_2014_web_final.pdf.

[23] HyET Solar. *Thin Film Composition*. url: https://www.hyetsolar.com/Thin-Film-Solar/thin-film-composition/.

[24] Robin Quax. "Fast and Smart Diagnostics for the monitoring and improvement of the production of a-Si:H modules on an industrial scale". Master's thesis. The Netherlands: TU Delft, 2013.

[25] HyET Solar. *HyET Solar Building*. url: https://www.hyetsolar.com/contact/.

[26] HyET Solar. *Powerfoil*. url: https://www.hyetsolar.com/powerfoil/.

[27] HyET Solar. *Production Process*. url: https://www.hyetsolar.com/production-process/.

[28] Top sector energie. *Delft University of Technology and HyET Solar. Project description. Flexible Lightweight Advanced Materials In Next Generation Of PV*. 2018. url: https://projecten.topsectorenergie.nl/projecten/flexible-lightweight-advanced-materials-in-next-generation-of-pv-31727.

[29] Arno Smets et al. *Solar Energy: The physics and engineering of photovoltaic conversion, technologies and systems*. English. UIT Cambridge Limited, 2016. isbn: 978-1-906860-32-5.

[30] R.B. Pettit et al. "Use of sol-gel thin films in solar applications". In: *Solar Energy Materials* 14 (1986), pp. 269–287.

[31] M.S. Kim, J.H. Lee, and M.K Kwak. "Surface Texturing Methods for Solar Cell Efficiency Enhancement". In: *Int. J. Precis. Eng. Manuf.* 21 (2020), pp. 1389–1398. doi: 10.1007/s12541-020-00337-5.

[32] Rath J. K. "Low temperature polycrystalline silicon: a review on deposition, physical properties and solar cell applications". In: *Sol. Energy Mater. Sol. Cells* 76 (2003), pp. 431–487.

[33] M. Joachim et al. "TCO and light trapping in silicon thin film solar cells". In: *Solar Energy* 77.6 (2004). Thin Film PV, pp. 917–930. issn: 0038-092X. doi: https://doi.org/10.1016/j.solener.2004.03.015. url: https://www.sciencedirect.com/science/article/pii/S0038092X04000647.

[34] A. A Yadav et al. "Electrical, structural and optical properties of SnO2:F thin films: effect of the substrate temperature." In: *J Alloys Compd* 488 (2009), pp. 350–355.

[35] H. L. Hartnagel et al. "Semiconducting Transparent Thin Films". In: *Institute of Physics* (1995).

[36] C. W. Tang and S. A. Van Slyke. In: *Appl. Phys. Lett.* 51 (1987), p. 913.

[37] M. Buchanan, J. B. Webb, and D. F. Williams. In: *Appl. Phys. Lett.* 37 (1980), p. 213.

[38] P Howson and H. A. Jafar. In: *J. Vac. Sci. Technol.* 10 (1992), p. 1784.

[39] T. Maruyama and K. Fukui. In: *Thin Solid Films* 203 (1991), p. 297.

[40] S. Kulaszewicz, W. Jarmoc, and K. Turowska. In: *Thin Solid Films* 112 (1984), p. 313.

[41] H. Kim et al. In: *J. Appl. Phys* 86 (1999), p. 6451.

[42] S. F. Tseng, W. T. Hsiao, and D. Chiang. "Mechanical and optoelectric properties of postannealed fluorine-doped tin oxide films by ultraviolet laser irradiation". In: *Appl. Surf. Sci.* 257 (2011), pp. 7204–7209.

[43] B. Thangaraju. "Structural and electrical studies on highly conducting spray deposited fluorine and antimony doped SnO2 thin films from SnCl2 precursor". In: *Thin Solid Films* 402 (2002), pp. 71–78.

[44] Lina S. S., Huanga J. L., and P. Sajgalik. “Effects of substrate temperature on the properties of heavily Al-doped ZnO films by simultaneous r.f. and d.c. magnetron sputtering Surface Coatings Technology”. In: 190 (2005), pp. 39–47.

[45] Rui L. et al. “Growth and properties of fluorine-doped tin oxide films deposited by ultrasonic spray pyrolysis”. In: *Journal of Plastic Film & Sheeting* 36.1 (2020), pp. 76–93. doi: 10.1177/8756087919846204.

[46] Wissal B. et al. “SnO2 Films Elaborated by Radio Frequency Magnetron Sputtering as Potential Transparent Conducting Oxides Alternative for Organic Solar Cells”. In: *ACS Applied Energy Materials* 5 (2022), pp. 170–177. doi: 10.1021/acsaem.1c02711.

[47] N. Chantarat et al. “Effect of Oxygen on the Microstructural Growth and Physical Properties of Transparent Conducting Fluorine-Doped Tin Oxide Thin Films Fabricated by the Spray Pyrolysis Method”. In: *ECS J. Solid State Sci. Technol.* 2 (2013), pp. 131–135.

[48] K. Zeng et al. “Investigation of Mechanical Properties of Transparent Conducting Oxide Thin Films”. In: *Thin Solid Films* 443 (2003), pp. 60–65.

[49] J. K. Yang et al. “Reference of Temperature and Time during Tempering Process for Non-Stoichiometric FTO Films”. In: *Sci. Rep.* 5 (2015).

[50] C. Hudaya, B. J. Jeon, and J. K. Lee. “High Thermal Performance of SnO2 :F Thin Transparent Heaters with Scattered Metal Nanodots”. In: *ACS Appl. Mater. Interfaces* 7 (2015), pp. 57–61.

[51] S. Wu et al. “Preparation, Characterization and Electrical Properties of fluorine-Doped Tin Dioxide Nanocrystals”. In: *J. Colloid Interface Sci.* 346 (2010), pp. 12–16.

[52] Y. Gassenbauer and A Klein. “Electronic and Chemical Properties of Tin-Doped Indium Oxide (ITO) Surfacesand ITO/ZnPc Interfaces Studied In-situ by Photoelectron Spectroscopy”. In: *J. Phys. Chem.* 110 (2006), pp. 4793–4801.

[53] X. H. hi and K. J. Xu. “Properties of Fluorine-Doped Tin Oxide Films Prepared by an Improved Sol-Gel Process”. In: *Mater. Sci. Semicond. Process.* 58 (2017), pp. 1–7.

[54] N. Memarian et al. “Characterization of SnO2 :F Thin Films Deposited by an Economic Spray Pyrolysis Technique”. In: *Solid state physics* 7 (2010), pp. 2277–2281.

[55] Ossila. *Innovation:Thin film solar cells at MX2016*. url: https://www.ossila.com/en-eu/pages/sheet-resistance-measurements-thin-films.

[56] Thermofisher Scientific. *Principles of scanning electron microscopy*. url: https://www.thermofisher.com/nl/en/home/materials-science/learning-center/applications/scanning-electron-microscope-sem-electron-column.html.

[57] Purdue University. *Scanning electron microscope*. url: https://www.purdue.edu/ehps/rem/laboratory/equipment%5C%20safety/Research%5C%20Equipment/sem.html.

[58] Hitachi. *Ultra-high Resolution Scanning Electron Microscope Regulus Series*. url: https://www.hitachi-hightech.com/global/product_detail/?pn=em-regulus.

[59] Hitachi Hitech. *Regulus Series FE-SEM*. url: https://www.hitachi-hightech.com/global/sinews/new_products/090501/.

[60] Pawley J .B. “Handbook of Biological Confocal Microscopy”. In: *Springer* (2006). doi: 10.1007/978-0-387-45524-2_1.

[61] Elliott A.D. “Confocal Microscopy: Principles and Modern Practices”. In: *Curr Protoc Cytom* 92 (2020). doi: 10.1002/cpcy.68.

[62] Stanford. *Microscopy: Keyence VK-X250/260K 3D Laser Scanning Confocal Microscope*. url: https://snsf.stanford.edu/facilities/fab/npc/keyence.

[63] Keyence. *Area Roughness Parameters*. url: https://www.keyence.eu/ss/products/microscope/roughness/surface/parameters.jsp.

[64] University of Twente. *VK 9700 KEYENCE*. url: https://www.utwente.nl/en/et/ms3/facilities/microscopy/VK%5C%209700%5C%20Keyence.

[65] UACJ Foil Corporation. *Bare Foil : UACJ Foil Corporation*. url: https://ufo.uacj-group.com/en/products/foil.html.

[66] How products are made. *How aluminum foil is made - material, manufacture, making, used, processing, dimensions, aluminium, procedure*. url: http://www.madehow.com/Volume-1/Aluminum-Foil.html..

[67] A. M. Shah. “Optimization Of Modulated Surface Texturing For Flexible Thin-Film Silicon Solar Cells”. Master’s thesis. The Netherlands: TU Delft, 2021.

[68] G. Hecht D. S; Hu; Irvin. “Emerging Transparent Electrodes Based on Thin Films of Carbon Nanotubes, Graphene and Metallic Nanostructures”. In: *Advanced Materials* 23(13) (2011), pp. 1482–1513.

[69] M. Tadatsugu. “Transparent conducting oxide semiconductors for transparent electrodes”. In: *Semiconductor Science and Technology* 60 (1986), S35.

[70] C.G. Granqvist I. Hamberg. “Evaporated Sn-doped In2O3 films: Basic optical properties and applications to energy-efficient windows”. In: *Journal of Applied Physics* 23(13) (1986), R123–R160.

[71] Chinmaya Rath. “Surface Characterization of Textured Al Foil for Thin Film Flexible Solar Cells”. Master’s thesis. The Netherlands: TU Delft, 2022.

[72] W. Perrin and W. H. Tarn. *CRC Handbook of metal etchants*. English. CRC Press LLC, 1991. isbn: 0-8493-3623-6.

[73] Microchemicals. *Aluminium etching*. 2013. url: https://www.microchemicals.com/technical_information/aluminium_etching.pdf.

[74] LLC ETCHANT STORE of ES Laboratory. *Nital etch test*. url: https://www.etchantstore.com/product-category/nital-etch-test/.

[75] Honda Electronic Co. Ltd. *Ultrasonics*. url: https://www.honda-el.net/ufile/library/2860_file.pdf.

[76] Products Finishing(PF). *Deoxidizing Aluminum as a Pretreatment*. url: https://www.microchemicals.com/technical_information/aluminium_etching.pdf.

[77] J. Wang, X. Shi, and W Liu. “Influence of Preferred Orientation on the Electrical Conductivity of Fluorine-Doped Tin Oxide Films”. In: *Sci Rep* 4 (2014), p. 3769. doi: 10.1038/srep03679.